Macromolecules

Article

pubs.acs.org/Macromolecules

Crystallization of Alternating Limonene Oxide/Carbon Dioxide Copolymers: Determination of the Crystal Structure of Stereocomplex Poly(limonene carbonate)

Finizia Auriemma,*[,†] Claudio De Rosa,[†] Maria Rosaria Di Caprio,[†] Rocco Di Girolamo,[†] and Geoffrey W. Coates[‡]

[†]Dipartimento di Scienze Chimiche, Università di Napoli "Federico II", Complesso di Monte S. Angelo, via Cintia, I-80126 Napoli, Italy

[‡]Baker Laboratory, Department of Chemistry and Chemical Biology, Cornell University, Ithaca, New York 14853-1301, United States

Supporting Information

ABSTRACT: The crystal structure of the alternating copolymer of limonene epoxide and carbon dioxide has been studied. Highly stereoregular and regioregular alternating copolymers have been prepared starting from cis/trans mixtures of both enantiopure (*R*) and (*S*) isomers of 1-methyl-4-(1-methylvinyl)-7-oxabicyclo[4.1.0] heptane (limonene oxide) using a *β*-diiminate zinc complex under mild conditions of temperature and pressure, to yield enantiopure poly(1*S*,2*S*,4*R*-limonene carbonate) (PRLC) and poly(1*R*,2*R*,4*S*-limonene carbonate) (PSLC) products, respectively. Attempts to crystallize the pure enatiomers failed, whereas racemic mixtures readily crystallize from solution, forming racemic crystals. In the crystals, enantiomorphic chains are packed in an orthorhombic unit cell with axes $a = 9.71 \pm 0.05$ Å, $b = 10.68 \pm 0.05$ Å, and $c = 11.31 \pm 0.05$ Å (chain axis) according to the space group $Pbc2_1$ and 2 chains (4 monomeric units)/unit cell. The chain periodicity *c* of 11.31 Å can be accounted for by a s(2/1) helical conformation with nearly all-trans bonds in the backbone. Isoclined chains of opposite chirality are packed in the unit cell forming well interdigitated *bc* layers piled along *a* via zipper interactions of the enantiomorphic side groups belonging to adjacent chains. The structure is characterized by the presence of different types and degrees of disorder that arises from the nearly random rotation of isopropenyl groups around the connection bond to the cyclohexane rings (conformational disorder), twisting of cyclohexane cycles, and up/down positional disorder of isochiral chains in the lattice positions (substitution type disorder). It is argued that the formation of racemic crystals instead of a mixture of enantiopure crystals is stabilized by the favorable interactions of the polar carboxyl groups and the zipper interactions of the lateral chiral groups of first neighboring chains along *b*. It is also inferred that the crystallization of enantiopure crystals is prevented by the slow crystallization kinetics and the less favorable interactions between chains in an isochiral packing.

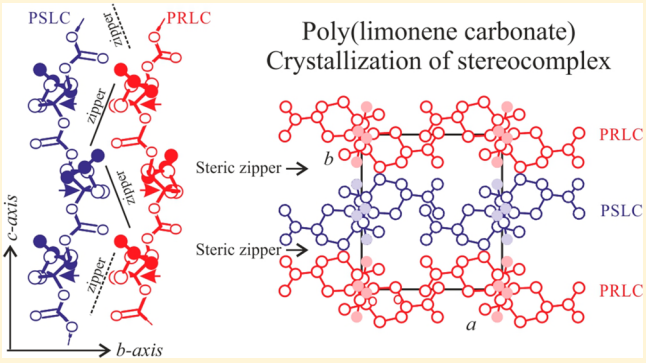

INTRODUCTION

Chirality in semicrystalline polymers is quite common. Although chiral polymers are typically constituted by chemical repeat units containing true asymmetric centers, they can also be formed from achiral monomers.[1] In fact, the helical conformations generally adopted by polymer chains in the crystals are intrinsically chiral, even though the chemical repeat is achiral.[2] This typically occurs for monomeric units presenting a stereoisomeric center which is not a true asymmetric carbon because it is linked to two undistinguishable chain segments, as in the case of stereoregular vinyl polymers $(-CH_2-C^*HR-)_n$.[2] For instance, isotactic vinyl polymers are chiral as long as the chain ends are distinguishable; in these polymers the chains adopt helical conformations, but right-handed and left-handed helices are equally probable since they are isoenergetic.[2] For this reason these polymers are called ***chiral but racemic***, where the chirality is buried, or cryptochiral.[1,3] Nonchiral (*chiral but racemic*) systems consisting of equally probable right and left-handed helices may crystallize either in nonchiral space groups where the helices of opposite handedness coexist in the unit cell in equal amount, or chiral space groups in which only helices of a given chirality are present in an individual polymer crystal. Of course, equal fractions of crystals of the enantiomorphous space groups will be present. In principle, the formation of chiral crystals from achiral or racemic helical polymers may be related to the stability of the chiral modification or may be associated with kinetic factors.[4,5] It has been suggested that a hexagonal or pseudohexagonal arrangement of helical chains in the

Received: January 27, 2015
Revised: March 21, 2015
Published: April 15, 2015

DOI: 10.1021/acs.macromol.5b00157
Macromolecules 2015, 48, 2534−2550

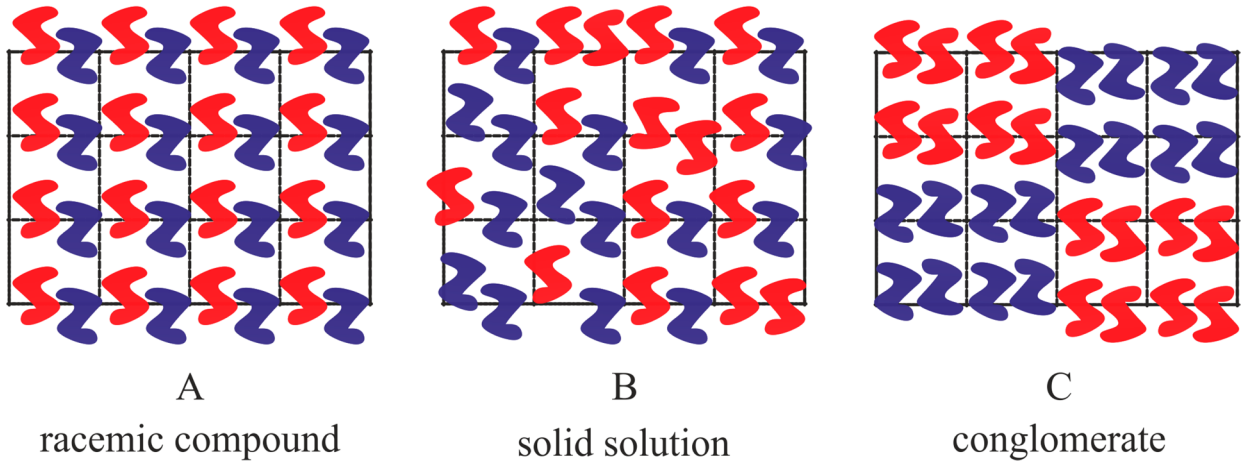

Figure 1. Optical compensation of racemic objects. (A) Compensation in a unit cell or racemic compound; (B) compensation in a crystallite or solid solution; (C) intercrystallite compensation or conglomerate; the case of mutual epitaxial growth of enantiomers is illustrated as an example, even though molecules of opposite chirality may also form well separated enanthiopure crystals.[15b] Structural units of opposite chirality (*R* = rectus and *S* = sinister) are indicated with different colors of Z and S shapes.

crystalline state promotes the chiral crystallization and is, in turn, favored by clustering of isochiral helices.[5] When a given polymer forms both chiral and nonchiral modifications, the nonchiral structure is often the most stable one, whereas the chiral form develops under kinetic control.[5]

In polymers characterized by truly chiral monomeric repeating units, that is monomers contain a "true" asymmetric atom, the chirality of the monomeric units favors the formation of helices of one specific chirality (right or left-handed). In fact, when the monomeric units are enantiomerically pure, helices of opposite chirality are not equivalent, since they have different conformational energies.[2b,c,4] This is for instance the case of isotactic poly((S)-3-methyl-1-pentene) iP(S)3MP, where only 4/1 left-handed helical chains are present in the tetragonal unit cell according to the space group $I4_1$.[6,7] Poly(L-peptides) and polylactides also fall in this class of chiral polymers. In particular, polylactides $[-C^*H(CH_3)-CO-O-]_n$ have a true asymmetry and can be obtained in the two enantiomorphic forms, poly(L-lactide) and poly(D-lactide) (PLLA and PDLA). Each species adopts a specific helicity, imposed by the stereochemistry, left-handed for poly(L-lactide) and right-handed for poly(D-lactide).[8−10]

Mixtures of enantiomeric polymers frequently give rise to macroscopic samples which are nonchiral, as these crystals are formed upon crystallization of a racemic mixture of chains having monomers with opposite absolute configurations. Enantiomorphic forms made of chains having monomers with opposite absolute configurations form helices of opposite hand and the two enantiomorphous helices are blended in the unit-cell of the racemic compound. Since monomers of opposite configurations occur in equal number, right and left-handed helical chains are equally probable. Unlike the case of ***chiral but racemic*** polymers, where the helices of opposite chirality may in principle interconvert, in this case the helices of opposite chirality are not isoenergetic and cannot interconvert.

This is the case, for instance, of the crystals of poly(L-lactide)/poly(D-lactide) stereocomplex, which forms upon crystallization of a racemic mixture of poly(L-lactide) and poly(D-lactide). In the crystals of the stereocomplex right-handed 3-fold helical chains of poly(D-lactide) and left-handed 3-fold helical chains of poly(L-lactide) are intrinsically blended in the trigonal unit cell, according to the space group *R*3*c* or $R\bar{3}c$.[11,12] Another example is provided by the form I of isotactic poly(*t*-butylethylene oxide), which presents chiral monomeric units giving two types of optical isomers, *rectus* (*R*) and *sinister* (*S*).[13] The tetragonal unit cell contains two left-handed 9/4 helical chains of the *rectus* polymer and two right-handed 9/4 helical chains of the *sinister* isomer,[13] giving a *racemic* compound and optical compensation.[14]

Optical compensation for polymers with chiral monomeric units may occur also when the racemic polymer consists of crystallites, each composed only of the rectus chains or only of the sinister polymer chains, and a same amount of optical antipodes crystallites are present. In general, for the various mentioned examples of racemic crystalline polymers where *R* and *S* polymers mix in a 1:1 ratio, three types of optical compensation shown in Figure 1 should be considered.[13,14] Optical compensation in a unit cell (**racemic compound**) is shown in Figure 1A, where the optical isomers are included in the unit cell pairwise. The compensation in a crystallite is shown in Figure 1B, where equal amount of *R* and *S* polymers are included in a crystallite randomly (**solid solution**), that is, they form a statistically disordered structure. The intercrystallite compensation (Figure 1C) is characterized by the presence of equal amounts of enantiomeric crystallites, each crystallite being composed only of *R* polymers or only of *S* polymers (**conglomerate**), and the bulk sample is optically inactive.[13,15] The intercrystallite optical compensation (Figure 1C)[14] has been found, for instance, in isotactic poly(propylene sulfide),[16] poly(*β*-methylpropriolactone),[17] and poly(isopropylethylene oxide),[18] where isochiral 2/1 helical chains are included in orthorhombic unit cells according to the space group $P2_12_12_1$. Another example of optical compensation in a unit cell (Figure 1A) is provided by isotactic poly(*tert*-butylethylene sulfide).[19]

Confining our attention to synthetic polymers whose chirality arise from the presence of true chiral atoms in the repeating unit,[1,3,4] we also mention the case of regio- and stereoregular alternating copolymers of carbon monoxide with propylene and other *α*-olefins with isotactic configuration in which the tertiary carbon atoms of only one kind of configuration, *R* or *S*, follow one each other in the backbone.[20] These alternating copolymers are able to crystallize either as enantiopure crystals or forming a racemic compound with melting temperature of the latter up to 100 °C higher than that

DOI: 10.1021/acs.macromol.5b00157
Macromolecules 2015, 48, 2534−2550

Chart 1. β-Diiminate Zinc Complex

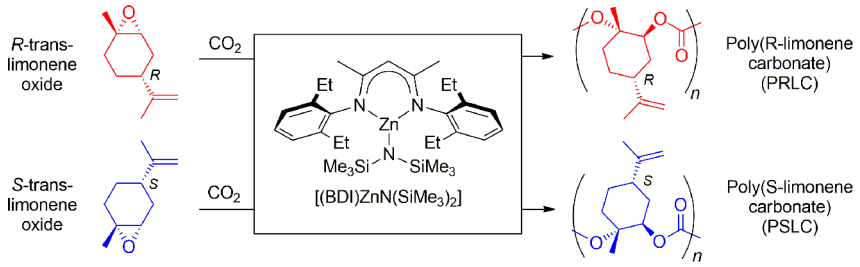

of enantipure crystals. In the case of poly(lactide) (PLA) the melting temperature of the stereocomplex is about 230 °C, that is ≈50 °C higher than that of the enantiopure crystals of the α-form.[11,12,21] In practice, in the cited examples, the pure enantiomers are able to crystallize forming enantiopure crystals, but in racemic mixtures the two optically active polymer chains components establish favorable interactions forming a stereocomplex[22] that behaves as a single macromolecule forming crystals with higher thermal resistance than the enantiopure crystals. It has been argued that this situation is created by stereoselective van der Waals interactions between chains of opposite chirality stabilizing the stereocomplex.[22]

In this paper the crystal structure of alternating copolymers of limonene oxide and carbon dioxide[23] of well-defined chirality obtained via regio- and stereo- selective polymerization of (*R*)- and (*S*)-limonene oxides with CO_2 is illustrated in detail. The corresponding pure enatiomers are the poly(1*S*,2*S*,4*R*-limonene carbonate) (PRLC) and the poly(1*R*,2*R*,4*S*-limonene carbonate) (PSLC), where the symbols R and S used in the abbreviated tags denote the chirality of the carbon atom linked to the isopropenyl substituent in each monomeric unit (*vide infra*). The two pure enantiomers have been obtained using a β-diiminate zinc complex as catalyst (Chart 1) at room temperature.[23] In a preliminary study,[24] we have shown that the pure enantiomers are not able to crystallize in spite of the highly regular constitution and configuration, but their racemic mixtures do easily crystallize thanks to formation of a stereocomplex. A structural model for the stereocomplex was also proposed, in which sheets of enantiopure chains intercalate with those of the opposite enantiomer, in a tight interdigitation.[24]

There is an intrinsic interest for this new class of biodegradable polymers, since they can be synthesized from completely renewable resources. Moreover the case of poly(limonene carbonate) represents an extreme example in polymer crystallography where favorable interaction of opposite enantiomers promote crystallization whereas crystallization of pure enantiomers is completely prevented. Here we report significantly more information about the crystal structure of the stereocomplex. The structural characterization is based on an in depth X-ray diffraction analysis, conformational and packing energy calculations and calculation of structure factors. Possible models of structural disorder in the conformation and packing of the chains are also discussed.

EXPERIMENTAL SECTION

Highly regio- and stereoregular poly(1*S*,2*S*,4*R*-limonene carbonate) (PRLC) and poly(1*R*,2*R*,4*S*-limonene carbonate) (PSLC) samples were prepared from *trans*/*cis*-*R*-limonene oxide (Sigma-Aldrich) and *trans*/*cis*-*S*-limonene oxide (Sigma-Aldrich), respectively, according to the literature method[23a] using the catalyst (BDI-Et_4)ZnN($SiMe_3$)$_2$. (Chart 1).[23b] The catalyst readily polymerizes the *trans* diastereomer of the epoxide, leaving the *cis* diastereomer unreacted, and resulting in a highly regio-, diastereo-, and enantiomerically pure polymer. Specific details regarding the polymer samples are given in the Supporting Information.

Stereocomplex polylimonene carbonate (PSLC/PRLC)[24] was prepared by dissolving equal amounts of PRLC (M_n = 59 000 g/mol) and PSLC (M_n = 50 500 g/mol) separately in hexanes (2.5 g/L). After filtering, the solutions were mixed, resulting in the immediate formation of a precipitate, in the shape of flakes, that was decanted and dried in vacuo. The ^{1}H and ^{13}C NMR spectra of PSLC/PRLC were identical to the spectra of PRLC (and PSLC).

We have examined the pure enantiomer PSLC and the racemic mixture PRLC/PSLC whose main characteristics are summarized in Table 1.

Table 1. Number Average Molecular Mass (M_n), Polydispersity Index (PDI), Glass Transition Temperature (T_g) and Degradation Temperature (T_D) of Poly(Limonene Carbonate) Samples PSLC and PRLC/PSLC[a]

sample	M_n[b]	PDI[b]	T_g[c] (°C)	T_D[c] (°C)
PSLC	78100[d]	1.1	122	247
PRLC/PSLC	59000[e]/50500[e]	1.1/1.2	122	261

[a]Synthesis are performed at 22 °C and 100 psi CO_2. [b]Determined by GPC analysis. [c]Determined by DSC and thermogravimettric analysis at heating rate of 10 °C/min. [d][epoxide]/[(BDI-Et_4)ZnN($SiMe_3$)$_2$] = 1000. [e][epoxide]/[(BDI-Et_4)ZnN($SiMe_3$)$_2$] = 500.

DSC scans and thermogravimetric measurements have been performed using a differential scanning calorimeter DSC Mettler 822 and a TA Instruments SDT 2960 thermo-balance, respectively in a flowing N_2 atmosphere at scanning rate 10 °C/min. The films used for structural analysis have been obtained by slow evaporation of the solvent from 3 wt % polymer solutions in tetrahydrofuran and methylene chloride. Crystalline films of PRLC/PSLC sample have been analyzed both before and after pulverization in order to randomize the orientation of crystallites using a cryogenic grinding mill.

X-ray diffraction patterns have been obtained with Ni-filtered Cu Kα radiation. The powder diffraction patterns have been obtained with an automatic Philips diffractometer, whereas the bidimensional diffraction patterns have been recorded on a BAS-MS imaging plate (FUJIFILM) using a cylindrical camera and processed with a digital imaging reader PERKIN ELMER CYCLONE PLUS (storage phosphor system).

Calculated structure factors have been obtained as $F_c = (\sum |F_i|^2 M_i)^{1/2}$, where F_i is the structure factor and M_i the multiplicity factor of the reflection i (Miller indices $(h\ k\ l)_i$) in powder diffraction patterns, and the summation is taken over all reflections included in the 2θ range of the corresponding diffraction peak observed in the X-ray powder diffraction profile. A thermal factor B = 8 Å^2 and atomic scattering factors as in ref 25 has been assumed.

The observed structure factors, F_0, have been evaluated from the intensities I_0 of the reflections observed in the powder diffraction profiles as $F_0 = (I_0/LP)^{1/2}$, where LP is the Lorentz-polarization factor for X-ray powder diffraction.[2c,26] The experimental intensities I_0 have

DOI: 10.1021/acs.macromol.5b00157
Macromolecules 2015, 48, 2534−2550

been evaluated by measuring the area of the peaks in the X-ray powder diffraction profile, after subtraction of a straight baseline approximating the background and of the amorphous contribution. For the amorphous profile the diffraction pattern of the pure enantiomer sample PSLC (or equivalently PRLC) has been used.

Simulated X-ray powder diffraction profiles and fiber diffraction patterns have been obtained with the software package[27] CERIUS^2, using the isotropic thermal factor B = 8 Å^2. For the calculation of powder diffraction data, profile functions having a half-height width regulated by the average crystallite size along a, b, and c axes, $L_a = L_b$ = 150 Å and L_c = 100 Å, respectively have been used. These values correspond to a coherence length along a, b, and c and are not true crystallite sizes. Simulated X-ray fiber diffraction patterns have been obtained fixing the half-width at half-height of crystallite orientation distribution (taken to be a Gaussian function centered on the fiber axis) equal to 9.7°.

Conformational energy calculations have been performed with the software package[27] CERIUS^2 using the force field PCFF[28] in the CERIUS program. For the conformational energy calculations on isolated molecules, a cutoff distance of 4 Å for attractive nonbonded interactions and for Coulombic interactions (dielectric constant, ϵ = 1) has been selected, and a spline function has been used from 4 to 5 Å to attenuate gradually the interaction energy from its full value to zero. No interaction over 5 Å was taken into account.

The packing energy has been evaluated as half the sum of the interaction energies between the atoms of one monomeric unit and all the surrounding atoms of neighboring macromolecules. The calculations of energy between non-bonded atoms have been performed using a 6−12 potential with the constants reported by Flory et al.[29] and taking the methyl groups as a single rigid unit (see Table S1). The conformation of the chain and the unit cell axes have been kept constant, and the interactions have been calculated within spheres of twice the sum of the van der Waals radii for each pair of atoms.

RESULTS AND DISCUSSION

The X-ray powder diffraction profile of the as prepared pure enantiomer PSLC is shown by curve a of Figure 2. The absence of Bragg reflections indicates that this sample is amorphous. The 1/1 mixture of the two pure enantiomers PSLC and PRLC precipitated from n-hexane solution, instead, is crystalline. This

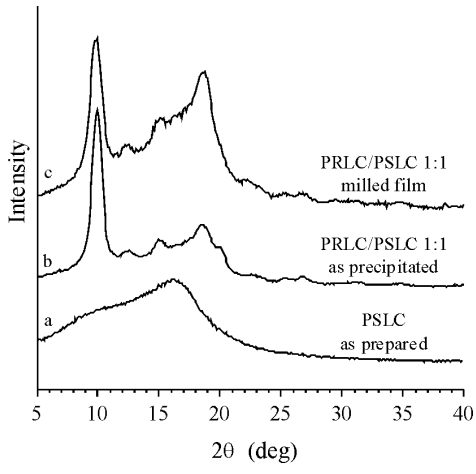

Figure 2. X-ray powder diffraction pattern of the pure enantiomer PSLC (a) and of the racemic mixture PRLC/PSLC (b, c) in the case of the as-prepared sample (a), flakes obtained by precipitation from n-hexane solution (b) and a powdered film obtained by casting from a 3 wt % tetrahydrofuran (THF) solution (curve a of Figure S2, Supporting Information) after milling in N_2(l) to randomize the orientation of the crystals.

is indicated by the X-ray powder diffraction profile b of Figure 2, which presents the main Bragg peaks at $d \approx$ 9.1, 7.3, 6.0, 5.6, 5.3, 4.8, and 4.5 Å ($2\theta \approx$ 9.7, 12, 15, 16, 16.6, 18 and 20°, respectively).

Attempts to crystallize the pure enantiomers PSLC or PRLC from solution either by precipitation or by solution casting procedures and/or annealing have resulted always in the formation of an amorphous sample, even using samples of low molecular mass (i.e., $M_n \approx 9.0 \times 10^3$ g/mol, entry **3** of ref 23a), whereas in the case of the racemic mixture a crystalline specimen is always obtained from solution also using different solvents. As an example, the X-ray powder diffraction profile of films obtained by dissolving the crystalline precipitate of the two enantiomers PRLC/PSLC at 3 wt % concentration in dichloromethane or tetrahydrofuran (THF), followed by casting on an aluminum substrate and successive slow evaporation of the solvent are shown in Figure S2, Supporting Information. The as-cast film presents Bragg peaks in the same positions as the crystalline flakes precipitated from hexane solution (curve b of Figure 2) with a marked predominance of the reflection at $d \approx$ 9.0 Å ($2\theta \approx$ 9.8°) (Figure S2). The tendency of the racemic mixture to form flakes or films with preferred orientation of the crystals is indicated by the fact that the relative intensity of these peaks changes after milling in N_2(l) obtaining X-ray powder diffraction profiles of the kind shown by curve c of Figure 2. The pulverized film, indeed, exhibits Bragg reflections in the same positions as the original film sample before grinding but the intensity distribution is completely changed (compare curves b and c of Figure 2).

As shown in ref 24, both samples show a glass transition temperature T_g of ≈122 °C and an endothermic peak at 247 °C in the case of the pure enantiomer and at 261 °C in the case of the racemic mixture. For both samples the DSC curves registered in the successive cooling scan is flat and we checked that no trace of sample is left in the DSC pan once back to room temperature. This indicates, as confirmed by thermogravimetric measurements, that the endothermic peaks at temperatures higher than 240 °C correspond to the degradation of the samples. Therefore, the melting temperature of the crystalline racemic mixture could not be observed, due to occurrence of degradation. We assume that the crystallinity observed in the case of the 1:1 mixture of the two enantiomers is due to the formation of a stereocomplex which crystallizes as a racemic compound (Figure 1A), rather than to the crystallization of the two enantiopure crystals forming a racemic conglomerate (Figure 1C) or a solid solution (Figure 1B). Formation of a stereocomplex is also inferred on the basis of the thermal stability of the racemate which is about 14 °C higher than that of the pure enantiomers.[22,24]

The presence of preferred orientation of the crystals in the as-cast films of the PRLC/PSLC racemate (Figure S2) turned out useful for the structural analysis. The bidimensional X-ray diffraction patterns taken using a cylindrical camera with the incident beam directed parallel to the film surface (with the normal to the film surface perpendicular to the axis of the cylindrical camera, edge direction, Figure 3A) is shown in Figure 3B, whereas the pattern obtained with the incident beam directed along the normal to the film surface (i.e., through the film, Figure 3C) is reported in Figure 3D. Whereas the X-ray diffraction pattern recorded in the through direction shows Debye−Scherrer rings with little or no polarization of Bragg reflections (Figure 3D), the X-ray diffraction pattern recorded in directions parallel to the film surface shows reflections that

DOI: 10.1021/acs.macromol.5b00157
Macromolecules 2015, 48, 2534−2550

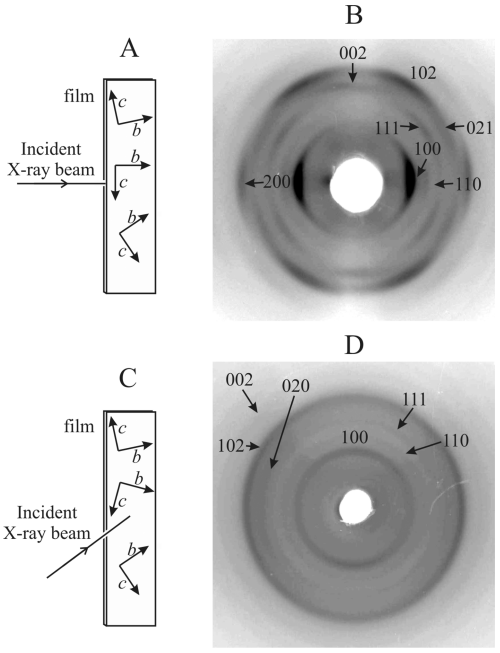

Figure 3. (B, D) Bidimensional X-ray diffraction pattern of a film of the racemic mixture obtained by casting from THF solution, collected using a cylindrical camera with the incident beam parallel to the film surface (the normal to the film is oriented horizontal, that is with *a** perpendicular to the surface) (A,B) and perpendicular to the film surface (the beam is directed parallel to the normal of film surface) (C,D). In parts A and C, the preferred orientation of (100) planes of the orthorhombic unit cell in the film plane is indicated, consisting in the orientation of the *a* axis parallel to the normal of film surface and the random orientation of the *b* and *c* axes in the plane of the film. In parts B and D, the *hkl* indices of reflections are also indicated.

Scheme 1. Chemical Constitution of Poly(1*S*,2*S*,4*R*-limonene carbonate) (PRLC) Chain (A) with Indication of the Relevant Dihedral Angles (A) and Chiralities in PSLC (B) and PRLC (C)

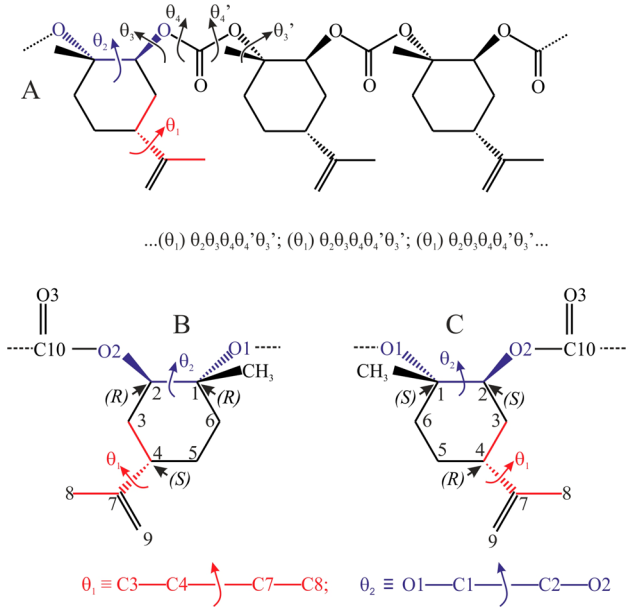

are polarized on well-defined layer lines (Figure 3B) corresponding to a layer periodicity of ≈11 Å.

Considering that the chain repetition unit of the stereoregular PRLC and PSLC chains in extended conformation is close to 11 Å (Scheme 1A) and includes two monomeric units per period, we assume that the *c*-axis of the crystals (parallel to the chain axis) lies in the plane of the film. A chain periodicity of ≈11 Å including two monomeric units/period is also in agreement with the presence in the pattern of Figure 3B of a strong meridional reflection on the second layer line. Moreover, in the X-ray diffraction pattern of Figure 3B, we distinguish three equatorial reflections at $d \approx 9.1$, 7.1, and 4.5 Å ($2\theta \approx 9.7$, 12 and 20°, respectively) two reflections polarized on the first layer line at $d = 6.0$ and 4.8 Å ($2\theta \approx 15$ and 18°, respectively) and two reflections on the second layer line at $d \approx 5.6$ Å (on the meridian) and 4.8 Å (off the meridian) ($2\theta \approx 16$ and 18°, respectively). The 2θ positions and Bragg distances of these reflections (Table 2) are in agreement with those observed in the X-ray powder diffraction profile of a milled film before (curve c of Figure 2) and after annealing (Figure 4, vide infra). The presence in the X-ray diffraction patterns recorded in the directions parallel to the film surface (Figure 3B) of a strong diffraction peak at $2\theta \approx 9.9°$ and of its second order at $2\theta \approx 20°$ localized on the equator along with the fact that these reflections are weak or absent in the X-ray diffraction pattern recorded in the through direction (Figure 3D) suggest the (*h*00) (alternatively (0*k*0)) uniplanar orientation of the crystals,[2c,30] which implies that the pole *a** (*b**) lies perpendicular to the film surface. We arbitrarily address this pole as *a**. This orientation corresponds to lamellar crystals grown edge on with respect to the film substrate, with the *a* axis (coincident with *a** axis in an orthorhombic unit cell) normal to the film surface and *b* and *c* axes laying in the plane of the film with random orientation.

The film of the PRLC/PSLC racemic mixture prepared by a casting procedure from THF solution (curve a of Figure S2) has been milled in N_2(l), (curve c of Figure 2) and successively annealed for 2 h at 180 °C and 45 min at 200 °C, obtaining the X-ray powder diffraction profile of Figure 4. This profile shows narrow and well resolved diffraction peaks that can be indexed according to an orthorhombic unit cell with parameters $a = 9.71 \pm 0.05$ Å, $b = 10.68 \pm 0.05$ Å, and $c = 11.31 \pm 0.05$ Å (chain axis). The calculated density, assuming 4 monomeric units in the unit cell (two chains), is 1.110 g/cm^3 in good agreement with the experimental value of crystalline density of the stereocomplex equal to 1.128 g/cm^3 (evaluated by flotation as described in the Supporting Information).

The *hkl* indices and the values of the 2θ positions and Bragg distances of the reflections observed in the X-ray diffraction profile of the PRLC/PSLC racemic sample of Figure 4 are compared in Table 2 with the calculated values. The reflections observed in the bidimentional diffraction pattern of Figure 3B relative to the film in the uniplanar orientation are also reported in Table 2. A satisfactory agreement between observed and calculated distances is obtained in the case of powdered specimen, whereas some differences are observed in the case of the oriented film due to the lower accuracy of measurements associated with the intrinsic broadness of reflections and the scarce degree of orientation of the crystals. Indeed, the proposed unit cell may not be the final one for this structure, but certainly will represent an important reference point for future refinements.

DOI: 10.1021/acs.macromol.5b00157
Macromolecules 2015, 48, 2534−2550

Table 2. Diffraction Angles ($2\theta_o$), Bragg Distances (d_o), Cylindrical Reciprocal Coordinates (ξ and ζ), and Intensities (I_o) of the Reflections Observed on the Layer Lines l of the X-ray Diffraction Pattern of Oriented Films of the PRLC/PSLC Racemic Mixture of Figure 3B, Compared with the Diffraction Angles, Bragg Distances, and Intensities of Reflections Observed in the X-ray Powder Diffraction Profile of Figure 4[a]

X-ray Diffraction Pattern of Oriented Films (Figure 3B)								
l	hkl	$2\theta_o$ (deg)	d_0 (Å)	ξ (Å^{-1})[b]	ζ (Å^{-1})[b]	$2\theta_c$ (deg)	d_c (Å)	I_o[b]
0	100	9.75	9.071	0.112	0	9.10	9.71	vvs
0	110	12.50	7.081	0.142	0	12.32	7.186	w
0	200	19.87	4.467	0.224	0	18.27	4.857	s
1	111	14.78	5.994	0.135	0.098	14.60	6.065	m
1	021	18.57	4.777	0.185	0.098	18.37	4.829	m
2	002	c	c	0	c	15.67	5.655	m
2	102	18.63	4.762	0.113	0.177	18.15	4.887	vs

X-ray Powder Diffraction of Unoriented Specimens (Figure 4)						
peak	hkl	$2\theta_o$ (deg)	d_0 (Å)	$2\theta_c$ (deg)	d_c (Å)	I_0
1	100	9.67	9.146	9.10	9.71	72.60
2	110	12.15	7.284	12.32	7.186	12.54
3	111	14.73	6.014	14.60	6.065	23.03
4	002	15.85	5.591	15.67	5.655	15.38
5	020	16.65	5.324	16.60	5.340	16.05
	102			18.15	4.887	
6	200	18.38	4.827	18.27	4.857	100.00
	021			18.37	4.829	
7	112	19.80	4.484	19.98	4.444	28.72
8	211	21.77	4.082	21.58	4.118	9.09
9	022	22.81	3.898	22.90	3.883	7.07
10	220	25.20	3.534	24.78	3.593	8.20
11	221	26.57	3.355	26.02	3.424	6.98
12	023	28.93	3.086	28.99	3.080	3.91
13	123	30.66	2.916	30.45	2.936	3.61
14	320	32.30	2.771	32.33	2.768	3.43
15	114	34.07	2.631	34.07	2.631	7.31
16	412	41.30	2.186	41.34	2.184	7.90
17	025	43.60	2.076	43.45	2.083	4.47

[a]The Miller indices of reflections and the values of diffraction angles ($2\theta_c$) and Bragg distances (d_c) calculated for the orthorhombic unit cell with axes a = 9.71 ± 0.05 Å, b = 10.68 ± 0.05 Å and c = 11.31 ± 0.05 Å are also indicated. [b]Values obtained by averaging over different patterns recorded with the incident beam parallel to the film surface according to the geometry of Figure 1B. (b) vvs=very very strong, vs=very strong, s=strong, m=medium, w=weak, (c) not determinable.

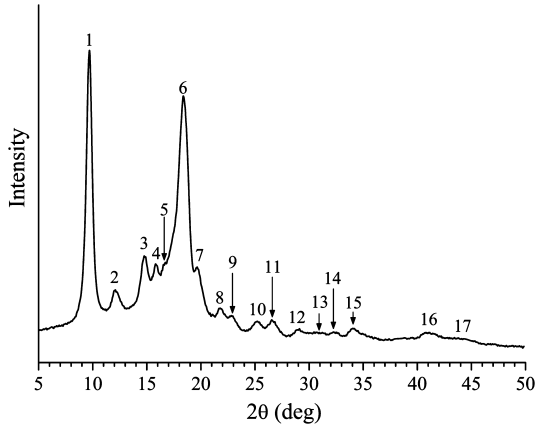

Figure 4. X-ray powder diffraction profile of the racemic mixture PRLC/PSLC obtained for a powdered film prepared by casting from THF solution after annealing at 180 °C for 2 h and 45 min at 200 °C. The Miller indices of the peaks are indicated in Table 2

MODEL CONFORMATIONS OF THE CHAIN FOR STRUCTURAL ANALYSIS

The constitution and configuration of the stereoregular PSLC and PRLC chains is compatible with the presence of a 2/1 helical axis parallel to the chain axis corresponding to the line repetition group **s**(2/1).[2c,31] This implies that the asymmetric unit coincides with the single monomeric unit, and identical repetition every two monomeric units. Therefore, once established the minimum energy conformation of the six membered rings and the values of torsion angles in a monomeric unit according to the succession $(\theta_1)\theta_2\theta_3\theta_4\theta_4'\theta_3'$ (see Scheme 1) with θ_1 defining the position of the pendant isopropenyl group with respect to the ring, the presence of the 2-fold helical axis entails the identical repetition of the conformational sequence of dihedral angles $[(\theta_1)\theta_2\theta_3\theta_4\theta_4'\theta_3']_n$ (Scheme 1A).

The repetition unit of PSLC and PRLC chains possess three chiral centers at C1, C2, and C4 carbon atoms, as indicated in Scheme 1B,C, and the symbols *S* and *R* in PSLC and PRLC

DOI: 10.1021/acs.macromol.5b00157
Macromolecules 2015, 48, 2534−2550

specify the chirality of the atom C4. For the sake of simplicity and without loss of generality we have fixed the geometry of the six-membered cyclohexane ring in the chair conformation. The opposite chirality of C_1 and C_4 carbon atoms belonging to the cycle (Scheme 1B,C) entails that the methyl and isopropenyl substituents are in trans with respect to the average plane of the ring, and therefore that they both are either in equatorial or axial positions. The chair conformation of the cyclohexane ring and the defined chirality of the monomeric units also implies that the torsion angle θ_2 external to the ring around the C1−C2 bond (i.e., O1−C1−C2−O2; see Scheme 1B,C) is gauche for the conformations with the methyl and isopropenyl groups in axial positions, and trans for the conformations with the two substituents in equatorial positions.

As a first step the methods of conformational analysis have been used to establish the values of the torsion angle θ_1 around the C4−C7 bond (defined according to the sequence C3−C4−C7−C8, Scheme 1B,C) corresponding to minimum energy conformations. The model monomers utilized for this analysis are the two enantiomeric diol compounds (1*S*,2*S*,4*R*)-4-isopropenyl-1-methyl-1,2-cyclohexanediol and (1*R*,2*R*,4*S*)-4-isopropenyl-1-methyl-1,2-cyclohexanediol (Figure 5). These

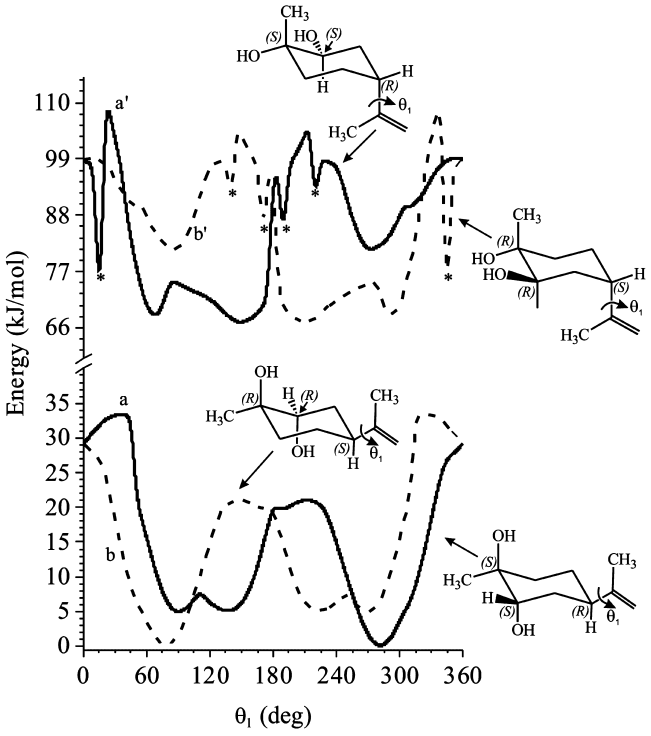

Figure 5. Conformational energy profiles of (1*S*,2*S*,4*R*)-4-isopropenyl-1-methyl-1,2-cyclohexanediol (a, a′) and (1*R*,2*R*,4*S*)-4-isopropenyl-1-methyl-1,2-cyclohexanediol (b, b′) with methyl and isopropenyl substituents at the C1 and C4 carbon atoms, respectively, in equatorial (a, b) and axial (a′, b′) positions. Asterisks indicate singular minima where large distortions of cyclohexane ring from chair conformation occur to alleviate unfavorable interactions between non-bonded atoms.

diols are obtained by alkaline hydrolysis of PRLC and PSLC samples, respectively.[23] Energy calculations have been performed as a function of θ_1 by minimizing the energy with respect to all remaining variables.

The results of energy calculations shown in Figure 5 indicate that energy minima correspond to conformers with the methyl and isopropenyl substituents in equatorial positions (curves a and b of Figure 5). In the case of (1*S*,2*S*,4*R*)-4-isopropenyl-1-methyl-1,2-cyclohexanediol with the methyl and isopropenyl substituents in equatorial positions (*R* isomer, curve a of Figure 5) absolute energy minimum is obtained at $\theta_1 = -80°$ and two additional broad minima only 4 kJ/mol higher than the absolute minimum are present at $\theta_1 = 90$ and 135°. In the case of the corresponding enantiomer (*S* isomer, curve b of Figure 5) energy minima occur for $\theta_1 = 80°$ (absolute minimum) −90° and −135°. The interconversion barrier between the different minima is of ≈20−30 kJ/mol. In the case of the conformers with the methyl and isopropenyl substituents in axial positions energy minima occur for $\theta_1 = +70°$, +150 and −85° for the *R* stereoisomer and $\theta_1 = -70°$, −150 and +85° for the *S* stereoisomer (curves a′ and b′, respectively, of Figure 5). However, the energy minima for the conformers with substituents in axial position are more than 60 kJ/mol higher than those with substituents in equatorial position. This indicates that the isopropenyl group lies in the equatorial position. Moreover, since the minima are broad a certain degree of conformational disorder with tendency of these substituents to oscillate around the minima is present along with a non null probability at room temperature to cross the conformational energy barriers separating the different minima. The minimum conformations of the model monomers found in our calculations is in good agreement with the conformation of (1*S*,2*S*,4*R*)-4-isopropenyl-1-methyl-1,2-cyclohexanediol in the crystalline state as established by single crystal X-ray diffraction analysis,[23a] indicating that the ring is in the chair conformation, the isopropenyl and methyl groups are in equatorial positions with $\theta_1 = 83°$.

Once established the minimum energy conformations for the lateral isopropenyl groups (i.e., the values of θ_1), energy calculations have been extended to models of dimers of Figure S3 in order to find a suitable conformation for the portions of chain connecting two consecutive rings in both PSLC and PRLC in the crystals. We have fixed the geometry of the rings in the chair conformation, the position of isopropenyl groups in one of the minima of Figure 5 (i.e., $\theta_1 = \pm 80°$, ∓ 90, and $\mp 135°$, for the conformers with the equatorial methyl and isopropenyl groups, $\theta_1 = \pm 70°$, ± 150, and $\mp 85°$ for the conformers with axial methyl and isopropenyl groups), a strict planarity of the carbonate groups with $\theta 4 \approx \theta 4'$ in the trans conformation.[32] The only left variables are the torsion angles around the C2−O2 bonds, $\theta 3$ and $\theta 3'$ (see Scheme 1). The results of these calculations, under the constraint of straight chain and identical conformation for the substituted cyclic groups, give a rather trivial result: low energy conformations with extended chain may be achieved only for the conformers with the methyl and isopropenyl groups in the equatorial positions regardless of the value of θ_1 and these conformation correspond to $\theta 3 \approx \theta 3'$ close to trans. In these conformers, the torsion angle θ_2 external to the ring around the C1−C2 bond is trans. In the case of the conformers with methyl and isopropenyl groups in the axial position, θ_2 is gauche and minimum energy conformations are obtained at high cost of energy with large distortions of the chair geometry of the ring toward twisted conformations and deviations of carbonate groups from planarity (i.e., $\theta_4 \approx \theta_4' = A^{\pm}$ with A denoting torsion angles deviating from ±120° within a range of ±30°).[31]

The above analysis allows building up low energy conformations for the chains of PRLC and PSLC in the crystals according to the **s**(2/1) line repetition group and periodicity *c* close to 11.3 Å. Examples of these conformations

DOI: 10.1021/acs.macromol.5b00157
Macromolecules 2015, 48, 2534−2550

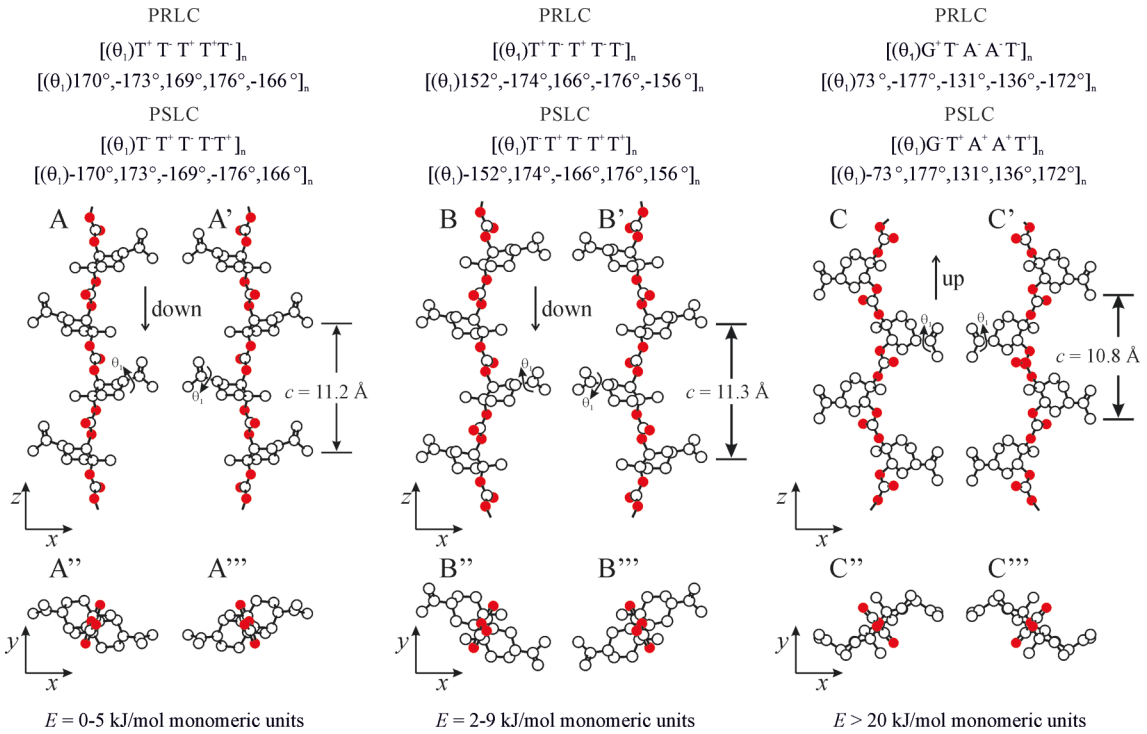

Figure 6. Low energy conformations of poly(1*S*,2*S*,4*R*-limonene carbonate) (PRLC) (A−C, A″−C″) and poly(1*R*,2*R*,4*S*-limonene carbonate) (PSLC) (A′−C′, A‴−C‴) according to the line repetition symmetry **s**(2/1), with indication of the values of torsion angles $\theta_2\theta_3\theta_4\theta_4'\theta_3'$ per monomer unit and θ_1 variable (defined in Scheme 1). The chain periodicity is also indicated: A−C, A′−C′, projections parallel to the chain axes; A″−C″, A‴−C‴, projections perpendicular to the chain axes. Chains in A,A′,B,B′ are down, with the bond connecting the quaternary carbon atom (C1 of Scheme 1B,C) to the tertiary carbon atom in the backbone (C2 of Scheme 1B,C) directed toward the negative direction of *z* axis; chains C,C′ are up, with the C1−C2 bond directed toward the positive direction of the *z* axis.

are shown in Figure 6. Low energy conformations correspond to chains with cyclohexane rings in the chair geometry, the methyl and isopropenyl substituents in equatorial position, all torsion angles in the backbone in the trans state and the dihedral angle θ_1 defining the position of the isopropenyl substituent variable in a wide range of values at low cost of internal energy defined by the minima of Figure 5. Examples of such low energy conformations are shown in Figure 6A,A′, B,B′ and they correspond to a succession of dihedral angles of the kind $[(\theta_1)\theta_2\theta_3\theta_4\theta_4'\theta_3']_n = [(\theta_1)T^+T^-T^+T^-T^-]_n$ for the R chain and $[(-\theta_1)T^-T^+T^-T^+T^+]_n$ for the S chain, with symbols T^+ and T^- indicating positive and negative deviations of torsion angles from 180° respectively of a quantity $|\delta| = 30°$, i.e., $T^+ = 180 - |\delta|$ and $T^- = 180 + |\delta|$.[31] The low energy conformation of parts A and B of Figure 6 are different due to a slight twisting of cyclohexane rings for the model of Figure 6B,B′, corresponding to a conformational energy cost less than 9 kJ/mol of monomeric units. Chain conformations characterized by the methyl and isopropenyl substituents in axial position and/or twisted geometries for the cyclohexane rings are also feasible at a relatively low cost of conformational energy of ≈20 kJ/mol of monomeric units. Such conformational models entail large deviations of the O−C−C−O backbone torsion angles θ_2 external to the ring from 180° toward gauche state and large deviations of the carbonyl groups from planarity (i.e., with $\theta_4 \approx \theta_4'$ close to $A^{\pm}$ states). An example of these higher energy conformations is shown in the structural model of Figure 6C,C′, corresponding to the succession of dihedral angles of the kind $[(\theta_1)\theta_2\theta_3\theta_4\theta_4'\theta_3']_n = [(\theta_1)G^+T^-A^-A^-T^-]_n$ for the R chain and $[(-\theta_1)G^-T^+A^+A^+T^+]_n$ for the S chain. For these models, under the geometrical restrain of s(2/1) line repetition group, the conformational energy decreases by allowing the chain periodicity to freely shrink from the experimental value of 11.3 Å to low values close to 9 Å.

It is worth noting from Figure 6 that the chains of poly(limonene carbonate) have a directional property consisting in the fact that the quaternary carbon atoms (C1 of Scheme 1B,C) may be connected to the tertiary carbon atom in the backbone (C2 of Scheme 1B,C) with the bond either pointing toward the positive direction of *z*-axis, or the negative direction, corresponding to "up" and "down" chain orientation. As an example the directionality of the models drawn in Figure 6A,A′B,B′ is down, and of the models of Figure 6C,C′ is up. We recall that chains with the same directionality are said isoclined whereas those with opposite directionality are said anticlined.[2c,31]

PACKING MODEL

Packing models have been built up while maintaining the maximum symmetry compatible with experimental data; i.e., the 2_1 helical axis of PRLC and PSLC chains is maintained as a crystallographic element of symmetry and only space groups of the orthorhombic crystal system have been considered. The presence of the strong 100 equatorial reflection at low 2θ value (i.e., $d = 9.15$ Å) and of the 111 reflection of medium intensity on the first layer line (at $d \approx 6$ Å) in the diffraction patterns of Figures 3B and 4 (see Table 2), suggests a packing mode of poly(limonene carbonate) chains with the chain axes positioned at (0 0 *z*) and ($0\ ^1/_2\ z$) of the unit cell.

Possible models of packing for poly(limonene carbonate) chains in **s**(2/1) symmetry in agreement with the above assumptions may correspond to the space groups $Pbc2_1$ and

DOI: 10.1021/acs.macromol.5b00157
Macromolecules 2015, 48, 2534−2550

$P22_12_1$. They are shown in Figure 7. The structural model of Figure 7A and space group $Pbc2_1$ is characterized by *ac* layers of

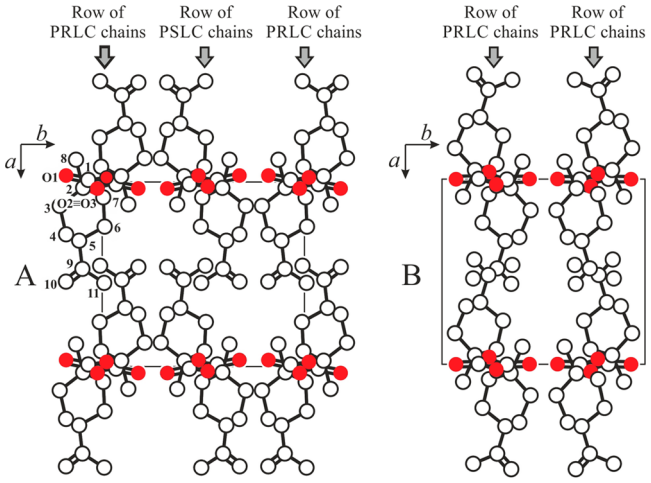

Figure 7. Structural models of the packing of poly(limonene carbonate) chains in the orthorhombic unit cell with axes a = 9.71 ± 0.05 Å, b = 10.68 ± 0.05 Å and c = 11.31 ± 0.05 Å (chain axis), according to the antichiral space group $Pbc2_1$ (A) and the chiral space group $P22_12_1$ (B) in projections perpendicular to the chain axes. Symbols "R" and "S" in PRLC and PSLC indicate the chirality of the tertiary carbon atom of the ring bearing the isopropenyl group in the case of poly(1*S*,2*S*,4*R*-limonene carbonate) and poly(1*R*,2*R*,4*S*-limonene carbonate) chains, respectively (see Scheme 1). In A, *ac* rows of isomorphous chains alternate along *b* with *ac* rows of chains of opposite chirality, and all chains are isoclined. In B, *ac* rows of isoclined chains alternate along *b* with *ac* rows of chains of opposite directionality and all chains are isochiral. In A the numbering scheme of the atoms of the asymmetric unit is indicated. The fractional coordinates of the atoms of the asymmetric unit are reported in Tables S4 and S5 of Supporting Information.

isoclined and isochiral chains alternating along *b* with *ac* layers of chains having the same directionality but opposite chirality. Therefore, this structural model includes two isoclined but enantiomorphic chains in the unit cell and is suitable for the description of racemic crystals stabilized by favorable interactions of PRLC and PSLC chains (Figure 1A). The structural model of Figure 7B and space group $P22_12_1$ is characterized by *ac* layers of isoclined, isochiral chains alternating along *b* with *ac* layers of chains having opposite directionality but the same chirality. Therefore, this structural model includes two anticlined and isomorphic chains in the unit cell and is suitable for the description of enantiopure crystals stabilized by favorable interactions of isochiral chains. This could imply that racemic mixtures of PRLC and PSLC chains crystallize from solution forming a racemic conglomerate rather than a racemic crystal (Figure 1C). In the latter hypothesis the fact that the pure enantiomers PRLC and PSLC are unable to crystallize in the same conditions in which the racemate crystallize could be possibly due to kinetic reasons.[33] For both space groups the asymmetric unit coincides with one monomeric unit, and the chain to which the asymmetric unit belongs is located at the origin for the antichiral space group $Pbc2_1$, at (0 $^1/_4$ z) for the isochiral space group $P22_12_1$.

The position of poly(limonene carbonate) chains in the unit cell have been found resorting to calculations of the potential energy interactions between non-bonded atoms belonging to adjacent chains while fixing the conformation of the chains (and therefore the chain periodicity) identical to those of the models of Figure 6B,B′, and varying the values of the torsion angle θ_1. Therefore, the packing energy has been calculated as a function of the value of the torsion angle θ_1 and of the variables that define the position of the chains in the unit cell corresponding to the degrees of freedom allowed by the symmetry of the space group. More precisely, for the antichiral packing mode according to the space group $Pbc2_1$ the only degree of freedom is the azimuthal setting of the chains, defined in Figure 8A by the clockwise rotation ω of the reference chain

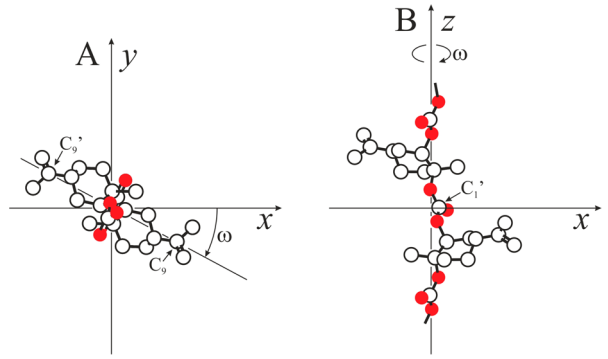

Figure 8. Definition of the structural variables used in the packing energy calculations to set the relative position of the chains in the unit cell. A: The azimuthal setting of the chains is defined by the clockwise rotation ω of the reference chain around the chain axis, with ω = 0 when the line connecting the atoms C9 and C9′ in the projection perpendicular to the chain axis coincides with the x-axis. B: The relative shift of the chains along the z-axis is defined by the z fractional coordinate of the carbonyl atom C1′ in the reference chain. The reference chain is placed at the origin for the space group $Pbc2_1$ (Figure 7A) and at (0 $^1/_4$ z) for the space group $P22_12_1$ (Figure 7B).

(at 0 0 z) around the chain axis. This angle is zero when the azimuthal setting of the reference chain is such that the in plane component of the line connecting the atoms C9 and C9′ belonging to the isopropenyl groups is aligned parallel to the *a*-axis of the unit cell (Figure 8A). For the isochiral space group $P22_12_1$, instead, two degrees of freedom are possible, corresponding to the azimuthal setting of the chains, defined as above by the rotation angle ω of the reference chain (at 0 $^1/_4$ z) around the own chain axis (Figure 8A), and the relative shift of the chains along z measured by the fractional coordinate z of the carbon atom of the carbonyl group C1′ of the reference chain (Figure 8B).

Results of these calculations are shown in Figures S5 and S6 and summarized in Tables S2 and S3. In the case of the antichiral space group $Pbc2_1$, for each conformer characterized by a different value of θ_1, the packing energy, calculated as a function of the azimuthal angle ω, is a periodic function of ω with period 180° (Figure S5), in agreement with the 2/1 helical symmetry of the chains. The energy profiles show, regardless of the value of θ_1, deep minima, ≈10° broad, for ω comprised in the range −10 to +10°, and 170−190° (Table S2). The calculated diffraction data for these models are in good agreement with experimental ones, regardless of the value of θ_1 and the exact conformation of the chain. In the case of the conformational model of Figure 6B, we have checked that the best agreement between calculated and experimental diffraction data corresponds to the structural model of Figure 7A with ω = 10° or 190° obtained by fixing the value of θ_1 = 317°. Therefore, this model corresponds to a low value of packing

DOI: 10.1021/acs.macromol.5b00157
Macromolecules 2015, 48, 2534−2550

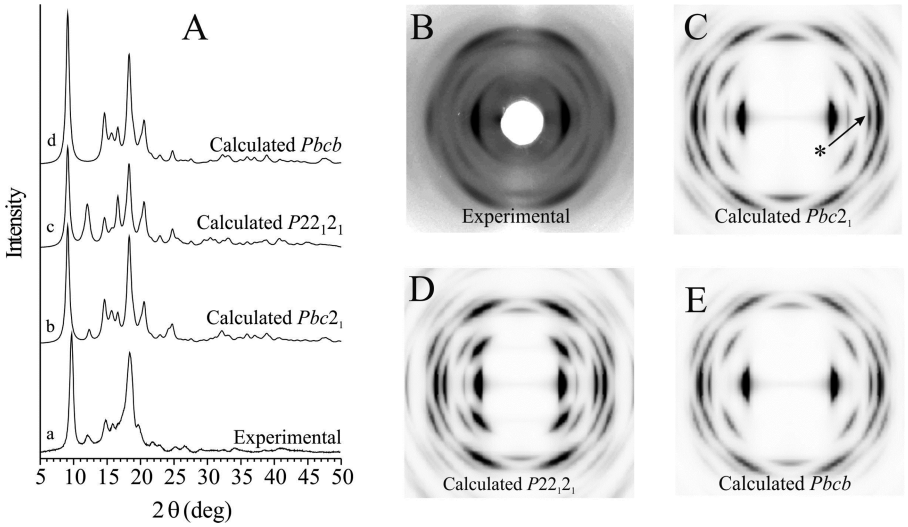

Figure 9. (A) Comparison of the experimental X-ray powder diffraction profile recorded for a film obtained by casting from THF solution of a PRLC/PSLC racemic mixture after milling in N_2(l) and successive annealing procedures (2 h at 180 °C and 45 min at 200 °C) (a), and calculated profiles relative to the limit ordered antichiral model corresponding to the space group $Pbc2_1$ (b), the limit ordered isochiral model corresponding to the space group $P22_12_1$ (c) and the limit disordered antichiral model corresponding to the space group *Pbcb* (d). (B–E) Comparison between the experimental bidimensional X-ray diffraction pattern (B) and those calculated for the limit ordered antichiral model $Pbc2_1$ (C), isochiral model $P22_12_1$ (D) and the limit disordered antichiral model *Pbcb* (E) structural models. The experimental profile a in A is the same as in Figure 4. The experimental diffraction pattern B has been recorded for an oriented film using a cylindrical camera (see Figure 3A), and it is the same as in Figure 3B. The 020 diffraction peak indicated with an asterisk in C is absent in the experimental pattern B due to the (*h*00) uniplanar orientation of the crystals for the film of PRLC/PSLC sample.

energy (Figure S5 and Table S2) and it is also of low conformational energy (Figure 6B).

The X-ray powder diffraction profile and the fiber diffraction pattern relative to the structural model of Figure 7A have been calculated using the utility "Diffraction-Crystal" of the Cerius[2] program and are compared in Figure 9 with the experimental diffraction data of the crystalline racemic mixture PRLC/PSLC (Figures 3B and 4). The main features of diffraction shown by the racemic mixture PRLC/PSLC crystallized from solution (profile a of Figure 9A and pattern of Figure 9B) are well reproduced in the simulated patterns (profile b of Figure 9A and pattern of Figure 9C). The fact that in the calculated two-dimensional diffraction pattern (Figure 9C) some reflection, as for instance the 020 diffraction peak indicated with an asterisk in Figure 9C, is absent in the experimental pattern of Figure 9B is due to the (*h*00) uniplanar orientation of the crystals for the film of the PRLC/PSLC sample, whereas the simulated pattern C has been calculated for a cylindrically symmetric distribution of the crystals around the *c*-axis. The comparison of experimental and calculated diffraction data in the case of the antichiral space group $Pbc2_1$ of Figure 9 indicates that the structural model of Figure 7A describes to a good approximation the crystal structure of the stereocomplex.

In the case of the isochiral space group $P22_12_1$, for each conformer characterized by a different value of θ_1, the packing energy has been calculated as a function of ω and z obtaining the contour maps of Figure S6. Also in this case the packing energy is a periodic function of ω and z with period 180° and $c/2$, respectively, in agreement with the 2/1 helical symmetry of the chains. As shown in Figure S6, deep and narrow minima are located at $\omega = 0 \pm 5°$ or $180 \pm 5°$, $z/c \approx 0.11$ or 0.61 regardless of the value of θ_1. The energy minima found for this isochiral model are reported in Table S3. All these minima are ≈2 kJ/mol of monomeric unit higher than the lowest minimum found for the antichiral model in the space group symmetry $Pbc2_1$. The absolute minimum of packing energy for the isochiral space group $P22_12_1$ occurs for the model shown in Figure 7B, characterized by $\theta_1 = 317°$, $\omega = 0°$ or 180°, and $z/c = 0.12$ or 0.62. The X-ray powder diffraction profile and the fiber diffraction pattern calculated for this model are shown in Figure 9, parts A (curve c) and D, respectively. Similar diffraction patterns would be obtained whatever the θ_1 value and the conformation of the chain. The scarce agreement between the experimental and calculated diffraction data for these isochiral models with isomorphous chains packed according to the space group $P22_12_1$ indicates that the non chiral structural models containing enantiomorphic chains packed according to the space group $Pbc2_1$ may be considered a better description for the crystal structure of PRLC/PSLC sample.

The values of the minima of packing energy calculated for the space groups $Pbc2_1$ and $P22_12_1$ as a function of θ_1 are compared in Figure 10. As shown in Tables S2 and S3 and discussed before, all minima occur for similar values of the azimuthal setting of chains, that is, roughly for values of ω around $5 \pm 10°$ or $175 \pm 10°$. The values of packing energy calculated in the case of the antichiral space group symmetry $Pbc2_1$ (curve a of Figure 10) are generally lower by at least 2 kJ/mol than those calculated for the isochiral packing model $P22_12_1$ (curve b of Figure 10), regardless of the value of θ_1, and only for θ_1 values around 60° and 230° the packing energy for the isochiral and antichiral packing modes becomes comparable. However, the energy barriers to be crossed for the interconversion between conformers with a different position of the pendant isopropenyl groups (i.e., θ_1 value) are less than 10 kJ/mol in the case of $Pbc2_1$ space group (curve a of Figure 10), and almost doubled in the case of the $P22_12_1$ space group (curve b of Figure 10). Since also the conformational energy barrier that allows for interchange between conformers with different values of θ_1 are not high (curves a, b of Figure 5), this suggests that the antichiral mode of packing of poly(limonene

DOI: 10.1021/acs.macromol.5b00157
Macromolecules 2015, 48, 2534–2550

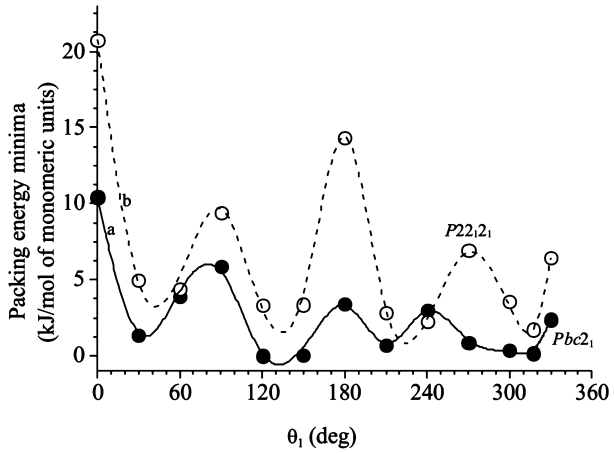

Figure 10. Values of packing energy minima (per mol of monomeric units) as a function of θ_1 relative to the antichiral packing mode of PRLC and PSLC chains according to the symmetry of the space group $Pbc2_1$ (a) and the isochiral space group symmetry $P22_12_1$ (b).

carbonate) chains appears better suited than the isochiral packing model to accommodate large amount of conformational disorder. Therefore, even if in principle the formation of enantiopure crystals would not be forbidden by the packing energy, the antichiral packing mode of PRLC and PSLC chains is favored not only energetically but also entropically.

A further insight into the proposed models for the packing of poly(limonene carbonate) chains comes from inspection of the *bc* projections of the models of Figure 7, shown in Figure 11. In this projection it is evident that in the case of the antichiral space group $Pbc2_1$ (Figure 11A) enantiomorphic chains with the same directionality are well interlocked with their chiral side groups in the (100) planes forming a kind of steric zipper (Figure 11A′), while maintaining the polar carbonyl groups at the same height along *z* and oriented toward the same direction (dashed lines of Figure 11A). The steric zipper occurs between chains of opposite chirality lying in adjacent *ac* planes along *b*, as shown in Figure 11A′. The bulky isopropenyl groups pending from the chiral carbon atoms of the rings in adjacent chains along *b* stick out from the planes parallel to *ac* alternatively in $+b$ and $-b$ directions, at *z* fractional coordinates z/c, $z/c + {}^1/_2$, $z/c + 1$ etc., so that they maximize their relative distance and produce a good interdigitation of atoms belonging to close neighboring chains (Figure 11A′).

In the case of the isochiral packing (Figure 11B), instead, this zipper mode interaction is not well established, the polar carbonyl groups and, hence, the chiral side groups belonging to adjacent chains are displaced each to other by $c/4$ along *z* (dashed line of Figure 11B), and the C═O bonds point toward opposite directions. We argue that the less favorable dipolar interactions of carbonyl groups prevent the crystallization of enantiopure crystals probably because the energy barrier for the formation of enantiopure crystals is too high. This barrier, instead, is low for the antichiral packing mode, and racemic crystals are formed more easily than enantiopure crystals for kinetic reasons. A low energy barrier for the formation of well-interlocked *bc* rows of chains, indeed, occurs for chain of opposite chirality, due to the very effective zipper of the antichiral chains and the favorable dipolar interactions of

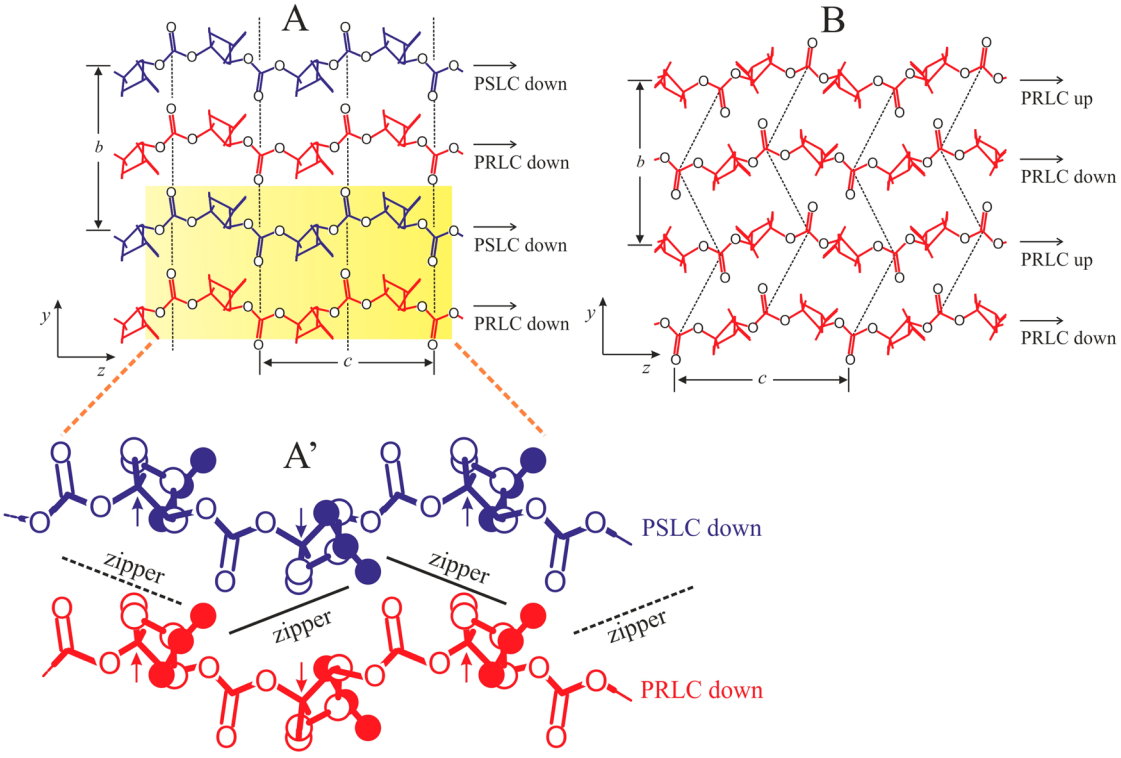

Figure 11. Packing models of poly(limonene carbonate) chains in an orthorhombic unit cell with axes a = 9.713 Å, b = 10.68 Å, c = 11.31 Å, and symmetry of the space group $Pbc2_1$ (A,A′) and $P22_12_1$ (B), in a projection perpendicular to the *a* axis. Isoclined chains (all up or all down) with opposite chirality alternate along *b* in A. Isomorphous chains with opposite up and down orientation alternate along *b* in B. The dashed lines connect consecutive carbonyl groups along *b*. In A′ the steric zipper between adjacent chains of opposite chirality along *b* is visualized in detail. Arrows in A′ point at quaternary carbon atoms C1 (see Scheme 1) in the backbone of *S* configuration in PRLC and *R* configuration in PSLC.

DOI: 10.1021/acs.macromol.5b00157
Macromolecules 2015, 48, 2534−2550

Table 3. Comparison between Observed Structure Factors (F_o), Evaluated from the X-ray Powder Diffraction Profile of Figure 4, and Calculated Structure Factors (F_{calc} and F_c) for the Models of Packing of Poly(limonene carbonate) of Figure 7A with θ_1 = 317° and ω = 10° in the Case of the Limit Ordered Model of Space Group Symmetry $Pbc2_1$, the Limit Disordered Model of Statistical Space Group Symmetry $Pbcb$, and for the Partially Disordered Model of Space Group Symmetry $Pbc2_1$ with Statistical Occupancy of Each Lattice Site of Isomorphous Chains Equal to 0.75 (or Equivalently 0.25) for Up Chains, 0.25 (or Equivalently 0.75) for Down Chains

Diffraction Peak	*hkl*	$2\theta_o$ (deg)	d_o (Å)	$2\theta_c$ (deg)	d_c (Å)	F_{calc}[a] $Pbc2_1$	$F_c/10$[b] $Pbc2_1$	F_{calc}[a] $Pbcb$	$F_c/10$[b] $Pbcb$	F_{calc}[a] $Pbc2_1$(dis)	$F_c/10$[b] $Pbc2_1$(dis)	$F_o/10$[c]
1	100	9.67	9.146	9.10	9.712	151.44	15	151.44	15	151.44	15	14
2	110	12.15	7.284	12.32	7.186	58.28	6	-	-	29.14	3	7
3	111	14.73	6.014	14.60	6.065	142.20	14	135.94	14	137.53	14	12
4	002	15.85	5.591	15.67	5.655	110.67	11	97.15	10	100.70	10	11
5	020	16.65	5.324	16.60	5.340	113.49	11	113.49	11	113.49	11	11
6	102 200 021 120	18.38	4.827	18.15 18.27 18.37 18.96	4.887 4.857 4.829 4.679	122.74 168.60 196.77 92.02	30	116.46 168.60 147.07 92.01	27	118.06 168.60 160.94 92.01	28	31
7	112 210 121	19.80	4.484	19.98 20.08 20.54	4.444 4.421 4.324	89.35 25.14 177.21	20	89.26 – 158.21	18	89.28 12.57 163.16	19	18
8	211	21.77	4.082	21.58	4.118	58.32	6	57.05	6	57.37	6	11
9	022	22.81	3.898	22.90	3.883	73.81	7	73.41	7	73.51	7	10
10	202 122 220 212	25.20	3.534	24.15 24.69 24.78 25.58	3.684 3.605 3.593 3.483	110.47 70.52 105.23 27.48	17	8.89 12.84 105.23 3.94	11	55.77 36.97 105.23 14.15	12	12
11	221 130 113 300 131	26.57	3.355	26.02 26.67 26.70 27.55 27.83	3.424 3.342 3.338 3.238 3.205	57.30 0.41 53.22 64.92 20.55	10	56.51 0.01 51.13 64.91 13.54	10	56.71 0.21 51.66 64.92 15.59	10	12
12	310 023 222 311	28.93	3.086	28.81 28.99 29.45 29.90	3.098 3.080 3.032 2.988	38.82 48.08 50.09 2.59	8	– 39.71 31.93 1.54	5	19.41 41.96 37.30 1.86	6	10
13	123 132 230 213	30.66	2.916	30.45 31.08 31.15 31.18	2.936 2.877 2.871 2.869	71.09 40.60 42.74 33.23	10	56.30 29.44 0.01 0.47	6	60.34 32.59 21.37 16.62	6	10
14	004 302 231 320 312 104	32.30	2.771	31.64 31.85 32.16 32.33 32.96 32.99	2.828 2.810 2.783 2.768 2.717 2.715	31.72 84.14 86.74 60.12 32.54 92.46	17	30.89 45.78 60.67 60.12 31.32 90.54	14	31.09 57.81 68.13 60.12 31.63 91.03	15	10

DOI: 10.1021/acs.macromol.5b00157
Macromolecules 2015, 48, 2534−2550

Table 3. continued

Diffraction Peak	*hkl*	$2\theta_o$ (deg)	d_o (Å)	$2\theta_c$ (deg)	d_c (Å)	F_{calc}[a] *Pbc*2_1	$F_c/10$[b] *Pbc*2_1	F_{calc}[a] *Pbcb*	$F_c/10$[b] *Pbcb*	F_{calc}[a] *Pbc*2_1(dis)	$F_c/10$[b] *Pbc*2_1(dis)	$F_o/10$[c]
15	321	34.07	2.631	33.32	2.689	75.08	21	68.21	17	69.99	18	16
	040			33.56	2.670	26.73		26.72		26.72		
	114			34.07	2.631	15.31		15.07		15.13		
	223			34.48	2.601	74.34		17.74		40.22		
	041			34.51	2.599	12.58		11.88		12.06		
	140			34.84	2.574	52.17		52.17		52.17		
	232			35.05	2.560	55.33		41.26		45.19		
	141			35.77	2.510	45.47		0.71		22.75		
	133			35.90	2.501	61.96		61.11		61.33		
	024			35.94	2.499	101.33		84.59		89.07		
	322			36.12	2.487	41.17		27.64		31.57		
	204			36.78	2.444	31.62		26.18		27.63		
	400			37.02	2.428	79.23		79.24		79.23		
n.o.[d]	124	-	-	37.15	2.420	75.71	8	51.06	5	58.21	6	-
n.o.[d]	042	-	-	37.24	2.414	13.03	1	3.78	0.4	7.30	0.7	-
n.o.[d]	330	-	-	37.55	2.395	22.72	2	0.01	<0.01	11.36	1	-
n.o.[d]	313	-	-	37.57	2.394	68.22	7	15.93	2	36.79	4	-
n.o.[d]	214	-	-	37.77	2.382	44.19	4	43.75	4	43.86	4	-
n.o.[d]	410	-	-	38.00	2.368	17.75	2	-	-	8.87	0.9	-
n.o.[d]	331	-	-	38.41	2.343	41.07	4	12.88	1	23.37	2	-
n.o.[d]	142	-	-	38.42	2.343	51.45	5	27.43	3	35.01	3	-
n.o.[d]	240	-	-	38.47	2.340	29.28	3	29.27	3	29.27	3	-
n.o.[d]	411	-	-	38.86	2.318	107.69	11	100.77	10	102.55	10	-
16	241	41.30	2.186	39.32	2.291	62.12	17	44.12	13	49.24	15	21
	233			39.45	2.284	57.78		38.99		44.44		
	323			40.42	2.231	37.27		25.55		28.93		
	402			40.42	2.231	65.14		20.61		37.14		
	224			40.60	2.222	14.16		6.04		8.80		
	420			40.82	2.210	63.94		63.94		63.94		
	332			40.92	2.206	15.01		11.76		12.66		
	412			41.34	2.184	40.72		38.69		39.21		
	043			41.44	2.179	37.73		32.95		34.21		
	421			41.63	2.169	23.41		23.23		23.27		
	242			41.78	2.162	10.53		9.62		9.85		
	134			41.85	2.159	37.59		13.24		22.02		
	115			41.87	2.158	50.16		34.56		39.05		
	304			42.44	2.130	20.98		20.27		20.45		
	143			42.52	2.126	68.45		67.11		67.44		

DOI: 10.1021/acs.macromol.5b00157
Macromolecules 2015, 48, 2534−2550

Table 3. continued

Diffraction Peak	*hkl*	$2\theta_o$ (deg)	d_o (Å)	$2\theta_c$ (deg)	d_c (Å)	F_{calc}[a] *Pbc*2_1	$F_c/10$[b] *Pbc*2_1	F_{calc}[a] *Pbcb*	$F_c/10$[b] *Pbcb*	F_{calc}[a] *Pbc*2_1(dis)	$F_c/10$[b] *Pbc*2_1(dis)	$F_o/10$[c]
17	314	43.60	2.076	43.32	2.089	35.34	13	3.32	10	17.90	11	17
	150			43.37	2.086	2.60		–		1.30		
	025			43.45	2.083	69.49		69.16		69.24		
	340			43.95	2.060	7.50		7.51		7.50		
	422			43.98	2.059	10.66		6.41		7.69		
	151			44.14	2.051	41.20		28.28		32.00		
	125			44.48	2.037	69.34		62.60		64.35		
	341			44.72	2.027	43.20		13.07		24.39		
	333			44.83	2.022	29.94		2.80		15.16		
	234			45.00	2.015	14.01		13.39		13.55		
	215			45.02	2.014	33.31		16.23		21.79		
	430			45.20	2.006	18.17		0.01		9.08		
	413			45.22	2.005	16.63		5.65		9.65		

[a]$F_{calc} = (F_i^2 \times M_i)^{1/2}$; [b]$F_c = (\Sigma F_{calc}^2)^{1/2}$, where the sum is extended over all reflections included in curly braces; [c]$F_0 = (I_o/LP)^{1/2}$; [d]Not observed.

carbonyl groups. These *bc* layers are the planes of maximum packing and act as the building blocks for the crystallization of poly(limonene carbonate) chains in racemic crystals. The fact that the formation of these building blocks should be quite easy due to the favorable interaction of the stereocomplex comes also from the consideration that the (100) planes are also the planes that are deposited parallel to the substrate upon crystallization of PRLC/PSLC racemic mixtures from solution by slow evaporation of the solvent.

STRUCTURE FACTOR CALCULATIONS

Structure factors have been calculated for the model of Figure 7A corresponding to the antichiral packing of poly(limonene carbonate) chains in low energy conformations of Figure 6B with $\theta_1 = 317°$, according to the space group *Pbc*2_1 for $\omega = 10°$. The fractional coordinates of the carbon and oxygen atoms of the asymmetric unit in the limit ordered model of Figure 7A are reported in the Supporting Information (Table S4). The calculated structure factors F_c are reported in Table 3 and compared with the observed structure factors F_0 evaluated from the experimental intensities observed in the X-ray powder diffraction profile of Figure 4 (Table 2).

A fairly good agreement between observed and calculated structure factors is obtained with a discrepancy factor *R* of 19% for the only observed reflections, whereas the discrepancy factor *R*′ calculated for both observed and non observed reflections is 24%. This indicates that the structural model of Figure 7A in the space group symmetry *Pbc*2_1 is a suitable description for the arrangement of poly(limonene carbonate) chains in the crystals, even though the structure factors of some reflections are calculated too high with respect to the observed ones. In particular, discrepancies are observed for the structure factors of the group of reflections in the region of $d = 2.3–2.4$ Å ($2\theta = 37–39°$), which are not observed, and the broad reflection at $d = 3.5$ Å ($2\theta \approx 25°$), which includes a too high contribution from the 202 reflection at $d \approx 3.7$ ($2\theta \approx 24.1°$). These discrepancies may be accounted for by the presence of conformational disorder due to the easy twisting of cyclohexane rings and the disorder in the position of the isopropenyl substituents (different values of θ_1), which namely affect the reflections at low Bragg distances. However, other kinds of structural disorder may also be present.

As an example, a kind of structural disorder that could affect the packing mode of poly(limonene carbonate) chains in the crystals may be envisaged in the presence of substitution type disorder,[2c] due to the statistical occupancy of up and down chains in the lattice positions. Such kind of disorder may be described in the short-range by the model of Figure 12A where *ac* rows of isomorphous and isoclined chains are piled along *b* with rows of chains of opposite chirality with probability *p* of maintaining the same directionality (as in the space group symmetry *Pbc*2_1) and probability (1-*p*) of assuming opposite directionality. In this model a strict alternation in the stacking along *b* of chains with opposite chirality is maintained. In Figure 12A, at the interface where a regular domain of all up (down) chains packed according to the space group *Pbc*2_1 meets a regular domain of all down (up) chains and space group *Pbc*2_1, the chains belonging to adjacent *ac* rows along *b* are characterized by identical azimuthal setting in order to keep the cost of interfacial energy low, thus disrupting the steric zipper established by enantiomorphic chains facing along *b* shown Figure 11A,A′. The short-range disorder of the structural model with *ac* rows of chains stacked with faults along *b* shown in Figure 12A with $p \geq 0.5$, may be described, in the long-range, by assuming that each lattice site in the structural model of Figure 7A and space group *Pbc*2_1 including all up (down) chains, may be statistically occupied by isomorphous chains that can be up (down) with probability *p*, or down (up) with probability $(1 - p)$. In the long-range, this model, for $p = (1 - p) = 0.5$, would correspond to the limit disordered model of packing described by the space group *Pbcb*, shown in Figure 12B, with *p* playing the role of an occupancy factor.

The structure factors have been calculated also for the limit disordered model in the space group *Pbcb* (Figure 12B) and compared with the experimental ones in Table 3. The fractional coordinates of the carbon and oxygen atoms of the asymmetric unit for the limit disordered model of Figure 12B are reported in the Supporting Information (Table S4), whereas the simulated X-ray diffraction profile and fiber pattern are included in Figure 9 (curve d of Figure 9A and pattern of Figure 9E).

DOI: 10.1021/acs.macromol.5b00157
Macromolecules 2015, 48, 2534–2550

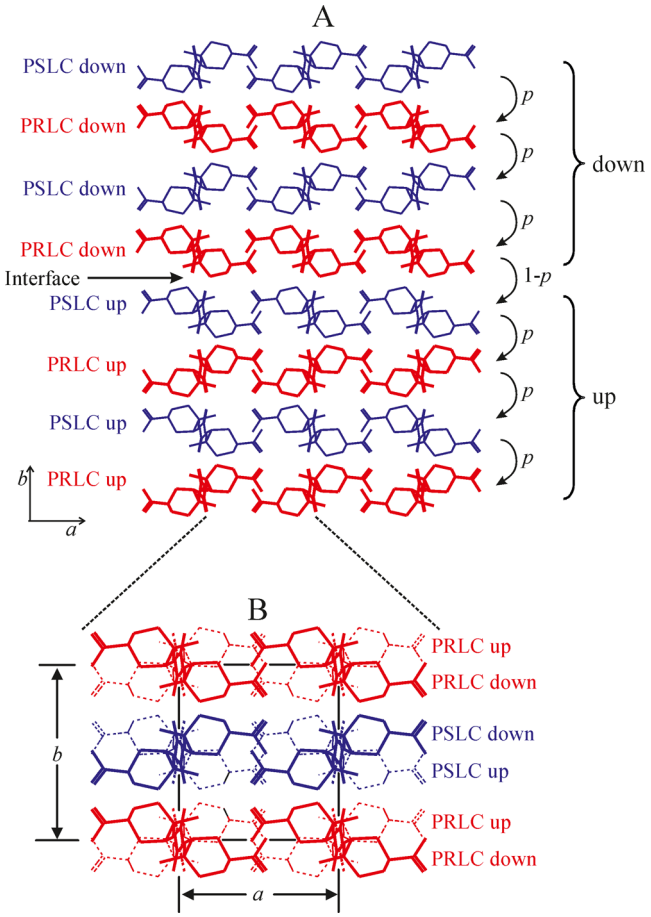

Figure 12. Disordered models for the packing of poly(limonene carbonate) chains in the crystals. (A) Model describing the disorder in the short-range, where *ac* rows of PRLC chains (thick lines) are piled along *b* with rows of PSLC chains (thin lines) with probability *p* of maintaining the same directionality (all up or all down) (as in the space group symmetry $Pbc2_1$) and probability $(1 - p)$ of assuming opposite directionality. At the interface where regular domains of all up and all down chains meet, the chains belonging to adjacent *ac* rows along *b* are characterized by identical azimuthal setting in order to keep the cost of packing energy low. (B) Limit disorder model describing the packing of poly(limonene carbonate) chains in the crystals in the long-range, corresponding to a statistical model with up and down chains of the same chirality statistically replacing each other in the lattice sites. The case $p = (1 - p) = 0.5$ corresponds to the space group symmetry *Pbcb*.

It is worth noting that for the space group *Pbcb* the presence of a glide plane symmetry *b* perpendicular to *c* axis implies the absence of *hk*0 reflection with *k* odd. As a consequence, the 110 reflection at $d \approx 7$ Å is calculated null in contrast with experimental data and also the disagreement factor increases to the values of $R = 24\%$ for the observed reflection and 28% for all reflections. However, the calculated structure factors of the 202 reflection at $d \approx 3.7$ ($2\theta \approx 24.1°$) and for the group of reflections in the region of $d = 2.3–2.4$ Å ($2\theta = 37–39°$) decrease (Table 3) in agreement with the experimental data. This suggests that disorder in the up/down arrangement of poly(limonene carbonate) chains in the crystals (Figure 12A) is probably present but only a certain degree of disorder is present. Partial degree of disorder cannot be described by the statistical space group *Pbcb* that implies a complete substitutional disorder of up and down chains in the sites of the lattice, but may be accounted for using, for instance, the model of stacking fault disorder of Figure 12A and assuming the probability $p > 0.5$. As an example, we have calculated the structure factor for a partially disordered model in the space group $Pbc2_1$ introducing an occupancy factor equal to 0.75 (or equivalently 0.25) for up chains and 0.25 (or equivalently 0.75) for down chains. The fractional coordinates and the occupancy factors of the atoms in the asymmetric unit and the structure factors for this partially disordered model and space group $Pbc2_1$ are reported in Tables S5 and 3, respectively. The disagreement factors for this disordered model are $R = 21\%$ for the observed reflections and $R' = 26\%$ for all reflections and are now only slightly higher than those relative to the limit ordered model $Pbc2_1$. Although the agreement with experimental data may be improved considering different conformational models for the chains such as the models of Figure 6, parts A and C, disorder in the azimuthal setting of chains, conformational disorder of side chains etc., our results indicate that a packing model containing two poly(limonene carbonate) isoclined chains of opposite chirality per unit cell packed according to the space group symmetry $Pbc2_1$ (Figure 7A) is a good description of the structure of the crystals obtained by slow evaporation of solvent from THF solutions of 1:1 mixture of PRLC and PSLC chains. The model of Figure 7A is, however, a limit ordered model structure. In fact, a high amount of conformational disorder is present in the crystals due to deviations of cyclohexane rings from the chair geometry toward twisted conformations, small deviations of backbone torsion angles from the *trans*-planar state and disorder in the position of isopropenyl groups associated with the low energy barrier around the C−C bond connecting the isopropenyl groups to the rings. Some amount of disorder in the lateral packing of chains is also present probably due to the disorder in the azimuthal setting of the chains in the crystals and a statistical occupancy of up and down chains in each site of the lattice.

■ CONCLUSIONS

The crystal structure of highly regio- and stereoregular poly(limonene carbonate) has been analyzed. This polymer is obtained from cheap and completely renewable resources using a *β*-diiminate zinc complex as catalyst able to promote the alternating copolymerization of CO_2 and (*R*)- or (*S*)-limonene-oxide yielding highly regio- and stereoregular poly-(1*S*,2*S*,4*R*-limonene carbonate) and poly(1*R*,2*R*,4*S*-limonene carbonate) (PRLS and PSLC), respectively. As prepared samples of the pure enantiomers are amorphous, present a glass transition temperature of ≈120 °C and a decomposition temperature of ≈250 °C.

Pure enantiomers are unable to crystallize under the normal crystallization conditions from solution, whereas crystalline powders are easily formed from solutions of 1:1 mixture of PRLC/PSLC components. The crystalline product shows a thermal degradation temperature ≈15 °C higher than the decomposition temperature of the pure enantiomers, indicating that the interactions between polymer segments of opposite chirality are preferred over the interactions between homochiral chains. This is considered the hallmark of formation of a stereocomplex.

Structural analysis has confirmed that PRLC and PSLC chains prefer to crystallize as racemic crystals rather than forming racemic conglomerates of enantiopure crystals. In these crystals couples of enantiomorphic and isoclined chains are packed in an orthorhombic unit cell with parameters *a* =

DOI: 10.1021/acs.macromol.5b00157
Macromolecules 2015, 48, 2534−2550

9.71 ± 0.05 Å, b = 10.68 ± 0.05 Å, and c = 11.31 ± 0.05 Å (chain axis) according to the space group $Pbc2_1$. Chains of opposite chirality alternate along b, according to a fish-bone arrangement with spine directed along a. The carbonyl groups are placed at the same height along z and are oriented toward the same direction. Crystallization is driven by the tight interdigitation of the side groups belonging to chains of opposite chirality along b and by favorable dipolar interactions. A high amount of conformational disorder is present, due to the easy twisting of cyclohexane rings and the low energy barrier of interconversion between different conformation energy minima around the bonds connecting the isopropenyl group to the ring, coupled with slight distortions of the backbone dihedral angles from trans-planar. A small amount of structural disorder is also present, due to the statistical occupancy of up and down chains in the lattice positions.

It is argued that the steric zipper established by the side groups belonging to poly(limonene carbonate) portions of chains with opposite chirality facing along b allows the easy crystallization of PRLC/PSLC mixture and the consequent formation of racemic crystals, whereas the crystallization of enantiopure crystals is kinetically prevented by the too high nucleation barrier namely due to less favored interactions between isochiral chain segments.

To our knowledge, the case of poly(limonene carbonate) is the first example of chiral polymers that in spite of the high degree of regio- and stereoregularity is unable to crystallize forming enantiopure crystals, but prefers to crystallize as stereocomplex.

■ ASSOCIATED CONTENT

Supporting Information

(1) Polymer synthesis, (2) additional X-ray diffraction data; (3) density measurements, (4) some geometrical and energy consideration on models of dimers, (5) packing energy calculations, and (6) fractional coordinates of atoms for the structural models of Figures 7A and 12B. This material is available free of charge via the Internet at http://pubs.acs.org.

■ AUTHOR INFORMATION

Corresponding Author

*(F.A.) Telephone: ++39 081 674341. Fax ++39 081 674090. E-mail: finizia.auriemma@unina.it.

Notes

The authors declare no competing financial interest.

■ ACKNOWLEDGMENTS

Financial support from MIUR (Project Prin 2010-2011) and the US National Science Foundation (CHE-1413862, CHE-1137345) is acknowledged.

■ REFERENCES

(1) (a) Okamoto, Y.; Nakano, T. *Chem. Rev.* **1994**, *94*, 349. (b) Farina, M. *Top. Stereochem.* **1987**, *17*, 1.

(2) (a) Corradini, P. In *The Stereochemistry of Macromolecules*, Ketley, A. D., Ed., Marcel Dekker, Inc.: New York, 1968, Vol. 3, p 1. (b) De Rosa, C. *Top. Stereochem.* **2003**, *24*, 71. (c) De Rosa, C.; Auriemma, F. *Crystals and Crystallinity in Polymers*; Wiley: Hoboken, NJ, 2014.

(3) (a) Mislow, K.; Bickart, P. *Israel J. Chem.* **1976/1977**, *15*, 1. (b) Mislow, K. *Collect. Czech. Chem. Commun.* **2003**, *68*, 849.

(4) Green, M. M.; Park, J.-W.; Sato, T.; Teramoto, A.; Lifson, S.; Selinger, R. L. B.; Selinger, J. V. *Angew. Chem., Int. Ed.* **1999**, *38*, 3138.

(5) Meille, S. V.; Allegra, G. *Macromolecules* **1995**, *28*, 7764.

(6) Corradini, P.; Petraccone, V.; Pirozzi, B. *Eur. Polym. J.* **1976**, *12*, 831.

(7) Petraccone, V.; Ganis, P.; Corradini, P.; Montagnoli, G. *Eur. Polym. J.* **1972**, *8*, 99.

(8) Puiggali, J.; Ikada, Y.; Tsuji, H.; Cartier, L.; Okihara, T.; Lotz, B. *Polymer* **2000**, *41*, 8921.

(9) (a) Hoogsteen, W.; Postema, A. R.; Pennings, A. J.; ten Brinke, G.; Zugenmaier, P. *Macromolecules* **1990**, *23*, 634. (b) De Santis, P.; Kovacs, J. *Biopolymers* **1968**, *6*, 299. (c) Miyata, T.; Masuko, T. *Polymer* **1997**, *38*, 4003. (d) Kobayashi, J.; Asahi, T.; Ichiki, M.; Okikawa, A.; Suzuki, H.; Watanabe, T.; Fukada, E.; Shikinami, Y. *J. Appl. Phys.* **1995**, *77*, 2957. (e) Aleman, C.; Lotz, B.; Puiggali, J. *Macromolecules* **2001**, *34*, 4795.

(10) Cartier, L.; Okihara, T.; Ikada, Y.; Tsuji, H.; Puiggali, J.; Lotz, B. *Polymer* **2000**, *41*, 8909.

(11) Cartier, L.; Okihara, T.; Lotz, B. *Macromolecules* **1997**, *30*, 6313.

(12) Okihara, T.; Tsuji, M.; Kawagushi, A.; Katayama, K. I.; Tsuji, H.; Hyon, S. H.; Ikada, Y. *J. Macromol. Sci. Phys.* **1991**, *B30*, 119.

(13) Sakakihara, H.; Takahashi, Y.; Tadokoro, H.; Oguni, N.; Tani, H. *Macromolecules* **1973**, *6*, 205.

(14) Tadokoro, H. *Polymer* **1984**, *25*, 147.

(15) (a) Jacques, J.; Collet, A.; Wilen, S. H. *Enantiomers, Racemates and Resolutions*; John Wiley & Sons: New York, 1981. (b) For low molecular mass compounds, crystallization of racemic conglomerates is a powerful approach in the preparation of enantiomerically pure compounds (Pasteur, L. C. R. *Hebd. Seance Acad. Sci. Paris* **1848**, *26*, 535). However, the resolution of racemic conglomerates by crystallization methods is often prevented by the formation of epitaxial racemic conglomerates (see for instance van Enckevort, W. J. P. *J. Chem. Phys.* **2010**,*114*, 21593; Srisanga, S.; ter Horst, J. H. *Cryst. Grow. Des.* **2010**, *10*, 1808). (c) Coquerel, G. *Top. Curr. Chem.* **2007**, *269*, 1.

(16) Sakakihara, H.; Chatani, Y.; Tadokoro, H.; Sigwalt, P.; Spassky, N. *Macromolecules* **1969**, *2*, 515.

(17) Yokouchi, M.; Chatani, Y.; Tadokoro, H.; Teranishi, K.; Tani, H. *Polymer* **1973**, *14*, 267.

(18) Takahashi, Y.; Tadokoro, H.; Hirano, T.; Sato, A.; Tsuruta, T. *J. Polym. Sci., Polym. Phys. Ed.* **1975**, *13*, 285.

(19) (a) Matsubayashi, H.; Chatani, Y.; Tadokoro, H.; Dumas, P.; Spassky, N.; Sigwalt, P. *Macromolecules* **1977**, *10*, 996. (b) Cartier, L.; Spassky, N.; Lotz, B. *C. R. Acad. Sci. Paris* **1996**, *322*, 429. (c) Cartier, L.; Spassky, N.; Lotz, B. *Macromolecules* **1998**, *31*, 3040.

(20) (a) Jiang, Z.; Adams, S. E.; Sen, A. *Macromolecules* **1994**, *27*, 2694. (b) Xu, F. Y.; Zhao, A. X.; Chien, J. C. W. *Makromol. Chem.* **1993**, *194*, 2579. (c) Sen, A. *Acc. Chem. Res.* **1993**, *26*, 303. (d) Sen, A.; Jiang, Z. *Polym. Mater. Sci. Ing.* **1992**, *67*, 102. (e) Brookhart, M.; Wagner, M. I. *J. Am. Chem. Soc.* **1994**, *116*, 3641. (f) Sen, A.; Jiang, Z. *Macromolecules* **1993**, *26*, 911. (g) Jiang, Z.; Boyer, M. T.; Sen, A. *J. Am. Chem. Soc.* **1997**, *117*, 7037. (h) Brückner, S.; De Rosa, C.; Corradini, P.; Porzio, W.; Musco, A. *Macromolecules* **1996**, *29*, 1535.

(21) (a) Lillie, E.; Schultz, R. C. *Makromol. Chem.* **1975**, *176*, 1901. (b) Kohn, F. E.; van den Berg, J. W. A.; van de Ridder, G.; Feijen, J. *J. Appl. Polym. Sci.* **1984**, *29*, 4265. (c) Tsuji, H. *Macromol. Biosci.* **2005**, *5*, 569. (d) Fukushima, K.; Kimura, Y. *Polym. Int.* **2006**, *55*, 626.

(22) (a) Slager, J.; Domb, A. J. *Adv. Drug. Del. Rev.* **2003**, *55*, 549. (b) Saravanan, M.; Domb, A. J. *Eur. J. Nanomed.* **2013**, *5*, 81.

(23) (a) Byrne, C. M.; Allen, S. D.; Lobkovsky, E. B.; Coates, G. W. *J. Am. Chem. Soc.* **2004**, *126*, 11404. (b) Cheng, M.; Moore, D. R.; Reczek, J. R.; Chamberlain, B. M.; Lobkovsky, E. B.; Coates, G. W. *J. Am. Chem. Soc.* **2001**, *123*, 8738.

(24) Auriemma, F.; De Rosa, C.; Di Caprio, M. R.; Di Girolamo, R.; Ellis, W. C.; Coates, G. W. *Angew. Chem., Int. Ed.* **2015**, *54*, 1215.

(25) Cromer, D. T.; Mann, J. B. *Acta Crystallogr.* **1968**, *A24*, 321.

(26) (a) Klug, H. P.; Alexander, L. E. *X-Ray Diffraction Procedures for Polycrystalline and Amorphous Materials*; Wiley-Interscience: New York, 1974;. (b) Buerger, M. J. *Crystal Structure Analysis*; John Wiley & Sons: New York, 1960.

(27) *Cerius*^{2} *Modeling Environment*; Molecular Simulations Inc.: San Diego, CA, 1999.

DOI: 10.1021/acs.macromol.5b00157
Macromolecules 2015, 48, 2534−2550

(28) (a) Dinur, U.; Hagler, A. T. New Approaches to Empirical Force Fields In *Review of Computational Chemistry*; **1991**; Chapter 4. (b) Maple, J. R.; Dinur, U.; Hagler, A. T. *Proc. Natl. Acad. Sci. U.S.A.* **1988**, *85*, 5350. (c) Sun, H.; Mumby, S. J.; Maple, J. R.; Hagler, A. T. *J. Am. Chem. Soc.* **1994**, *116*, 2978. (d) Sun, H. *Macromolecules* **1994**, *26*, 5942. (e) Sun, H. *Macromolecules* **1995**, *28*, 701.
(29) (a) Yoon, D. Y.; Sundararajan, P. R.; Flory, P. J. *Macromolecules* **1975**, *8*, 776. Sundararajan, P. R.; Flory, P. J. *J. Am. Chem. Soc.* **1974**, *96*, 5025. (b) Vacatello, M.; Flory, P. J. *Macromolecules* **1986**, *19*, 405.
(30) (a) Alexander, L. E. *X-ray Diffraction Methods in Polymer Science*; R. E. Krieger Publishing Company: Huntington, NY, 1979;. (b) Heffelfinger, C. J.; Burton, R. L. *J. Polym. Sci.* **1960**, *47*, 289.
(31) (a) Meille, S. V.; Allegra, G.; Geil, P. H.; He, J.; Hess, J.; Jin, J.-I.; Kratochvíl, P.; Mormann, W.; Stepto, R. *Pure Appl. Chem.* **2011**, *83*, 1831−1871. (b) Allegra, G.; Corradini, P.; Elias, H. G.; Geil, P. H.; Keith, H. D.; Wunderlich, B. *Pure Appl. Chem.* **1989**, *61*, 769.
(32) Williams, A. D.; Flory, P. J. *J. Polym. Sci., Part A-2* **1968**, *6*, 1945.
(33) Brock, C. P.; Schweizer, W. B.; Dunitz, J. D. *J. Am. Chem. Soc.* **1991**, *113*, 9811.

DOI: 10.1021/acs.macromol.5b00157
Macromolecules 2015, 48, 2534−2550